TEZ ŞABLONU ONAY FORMU
THESIS TEMPLATE CONFIRMATION FORM

1. Şablonda verilen yerleşim ve boşluklar değiştirilmemelidir.
2. Jüri tarihi, Başlık Sayfası, İmza Sayfası, Abstract ve Öz'de ilgili yerlere yazılmalıdır.
3. İmza sayfasında jüri üyelerinin unvanları doğru olarak yazılmalıdır. Tüm imzalar **mavi pilot kalemle** atılmalıdır.
4. Tezin **son sayfasının sayfa numarası** Abstract ve Öz'de ilgili yerlere yazılmalıdır.
5. Bütün chapterlar, referanslar, ekler ve CV sağ sayfada başlamalıdır. Bunun için **kesmeler** kullanılmıştır. **Kesmelerin kayması** fazladan boş sayfaların oluşmasına sebep olabilir. Bu gibi durumlarda paragraf (¶) işaretine tıklayarak kesmeleri görünür hale getirin ve yerlerini **kontrol edin**.
6. Figürler ve tablolar kenar boşluklarına taşmamalıdır.
7. Şablonda yorum olarak eklenen uyarılar dikkatle okunmalı ve uygulanmalıdır.
8. Tez yazdırılmadan önce PDF olarak kaydedilmelidir. Şablonda yorum olarak eklenen uyarılar PDF dokümanında yer almamalıdır.
9. **Bu form aracılığıyla oluşturulan PDF dosyasını arkalı-önlü yazdırın.**
10. Tez taslağınız, ilgili alanları (jüri imzalandıktan sonra, Tez Juri Atama Formu ile birlikte Lisansüstü Akademik Kurul Sekreterliğine teslim edilmelidir.
11. Tez taslaklarının kontrol işlemleri tamamlandığında, bu durum öğrencilere METU uzantılı öğrenci e-posta adresleri aracılığıyla duyurulacaktır.

1. Do not change the spacing and placement in the template.
2. Write defence date to the related places given on Title page, Approval page, Abstract and Öz.
3. Write the titles of the examining committee members correctly on the Approval Page. **Blue ink** must be used for all signatures.
4. Write **the page number of the last page** in the related places given on Abstract and Öz pages.
5. All chapters, references, appendices and CV must be started on the right page. **Section Breaks** were used for this. **Change in the placement** of section breaks can result in extra blank pages. In such cases, make the section breaks visible by clicking the paragraph (¶) mark and **check their position.**
6. All figures and tables must be given inside the page margins. Nothing must appear in the margins.
7. All the warnings given in the comments section through the thesis template must be read and applied.
8. Save your thesis as pdf and Disable all the comments before taking the printout.
9. **Print two-sided the PDF file that you have created through this form.**
10. Once you have signed the relevant fields in your thesis draft, submit it to the department secretary together with your Thesis Jury Appointment Form.
11. This will be announced to the students via their METU students e-mail addresses when the control of the thesis drafts has been completed.

☒ **Yukarıda bulunan tüm maddeleri okudum, anladım ve kabul ediyorum. / I have read, understand and accept all of the items above.**

Name : Muhammad
Surname : Musadiq
E-Mail : Muhammad.musadiq@metu.edu.tr
Date : 1/07/2022
Signature : _____

INCREASING THE RELIABILITY OF THE POWER CONVERTERS USED IN RENEWABLE ENERGY SYSTEMS BY USING A VARIABLE SWITCHING ALGORITHM

A THESIS SUBMITTED TO
THE BOARD OF GRADUATE PROGRAMS
OF
MIDDLE EAST TECHNICAL UNIVERSITY, NORTHERN CYPRUS CAMPUS

BY

MUHAMMAD MUSADIQ

IN PARTIAL FULFILLMENT OF THE REQUIREMENTS
FOR
THE DEGREE OF MASTER OF SCIENCE
IN ELECTRICAL AND ELECTRONICS ENGINEERING PROGRAM

JULY 2022

Approval of the Board of Graduate Programs

Prof. Dr. Cumali Sabah

Chairperson

I certify that this thesis satisfies all the requirements as a thesis for the degree of Master of Science

Assoc. Prof. Dr. Murat Fahrioğlu

Program Coordinator

This is to certify that we have read this thesis and that in our opinion it is fully adequate, in scope and quality, as a thesis for the degree of Master of Science.

Asst. Prof. Dr. Canras Batunlu

Supervisor

Examining Committee Members

Asst. Prof. Dr. Mehmet Şenol	Electrical and Electronics Engineering Program CIU _____
Assoc. Prof. Dr. Tayfun Nesimoglu	Electrical and Electronics Engineering Program METU NCC _____
Asst. Prof. Dr. Canraş Batunlu	Electrical and Electronics Engineering Program METU NCC _____

I hereby declare that all information in this document has been obtained and presented in accordance with academic rules and ethical conduct. I also declare that, as required by these rules and conduct, I have fully cited and referenced all material and results that are not original to this work.

Name, Last name: Muhammad, Musadiq

Signature:

ABSTRACT

INCREASING THE RELIABILITY OF THE POWER CONVERTERS USED IN RENEWABLE ENERGY SYSTEMS BY USING A VARIABLE SWITCHING ALGORITHM

Musadiq, Muhammad
Master of Science, Electrical and Electronics Engineering Program
Supervisor: Asst. Prof. Dr. Canras Batunlu

July 2022, 91 pages

As we recognize that the number of people on earth is growing at an exponential rate, so does the energy demand, if producing power from wind and solar is contemplated, resources can be used to meet that demand. The purpose of this thesis is to design a converter that helps to integrate the renewables into the DC Microgrid smoothly and encounters the thermal issues on its own. To avoid these circumstances' reliability of the power converters increased by reducing the temperature issues and the thermal variation which occurs due to changes in operating conditions and for this variable switching and variable inductance technique has been applied in the system.

In this thesis, a system is built to perform the simulation concerning real environmental conditions. The system is consisting of a condition monitoring unit which will monitor failure indicators and there will be an active thermal control unit which will control the temperature of the converter with the help of switching techniques. The methodology has been applied for various switching frequencies for the power electronic DC-DC converter. The lifetime consumption outcome at 5kHz without controller 4.75928 x 10-96 and without controller 2.65298 x 10-95. The outcome at 10kHz without controller 4.75928 x 10-96 and with controller 1.75285 x 10-95. By analyzing the results, it can be concluded that the overall reliability of the converter is increasing with the increase in frequency.

Keywords: Micro-grid, Active thermal unit, Power converters, Switching Algorithms

ÖZ

DEĞİŞKEN ANAHTARLAMA ALGORİTMASI KULLANARAK YENİLENEBİLİR ENERJİ SİSTEMLERİNDE KULLANILAN GÜÇ KONVERTÖRLERİNİN GÜVENİLİRLİĞİNİN ARTIRILMASI

Musadik, Muhammed
Yüksek Lisans, Elektrik ve Elektronik Mühendisliği
Tez Yöneticisi: Dr. Öğr. Üyesi. Canras Batunlu

Temmuz 2022, 91 sayfa

Rüzgar ve güneş enerjisi kullanılarak elektrik üretmek düşünüldüğünde, dünyanın çok fazla potansiyeli olduğu ve bu talebi karşılamak için rüzgar ve güneş enerjisi kaynaklarının kullanılabilir olduğu öngörülmektedir. Bu tezin amacı, yenilenebilir enerjiyi, DC Mikro şebekeye sorunsuz bir şekilde entegre etmeye yardımcı olan ve termal sorunları kendi başına karşılayan bir dönüştürücü tasarlamaktır. Bu durumlardan kaçınmak için, sıcaklık sorunları ve çalışma koşullarındaki değişiklikler nedeniyle oluşan termal değişim azaltılarak güç dönüştürücülerinin güvenilirliği artırılmış ve bu değişken anahtarlama ve değişken endüktans tekniği sistemde uygulanmıştır. Bu tezde, gerçek çevre koşulları ile ilgili simülasyonu gerçekleştirmek için bir sistem kurulmuştur. Sistem, arıza göstergelerini izleyecek durum izleme ünitesinden oluşmakta olup, konvertörün sıcaklığını anahtarlama teknikleri yardımıyla kontrol edecek aktif termal kontrol ünitesi geliştirilmiştir. Metodoloji, güç elektroniği DC-DC dönüştürücü için çeşitli anahtarlama frekansları için uygulanmıştır. 5kHz'de çalışan sistem için, oluşturulan kontrolör ile 4.75928 x 10-96 ve kontrolör olmadan 2.65298 x 10-95 ömür süresi tüketim sonucu elde edilmiştir. 10kHz'de çalışan dönüştürücü modelinde, kontrolör ile 4.75928 x 10-96 ve kontrolör olmadan 1.75285 x 10-95 ömür süresi tüketim sonucu elde edilmiştir. Sonuçları analiz ederek, çalışma frekansındaki artışla, dönüştürücünün genel güvenilirliğinin arttığı sonucuna varılabilir.

Anahtar Kelimeler: Mikro şebeke, Aktif termik ünite, Güç dönüştürücüler, Anahtarlama Algoritmaları.

First of All, I want to dedicate this success to Almighty Allah, who make me capable to complete my studies in a best possible way, then my parents (Muhammad Siddiq Ahmed Dawood and Fatima Siddiq) and siblings (Muhammad Bilal Siddiq and Mirha Siddiq) for their immense support and prayers.

ACKNOWLEDGMENTS

Firstly, all thanks to Allah Almighty for his countless blessings because without them it won't be possible at any cost. It is his blessing that I can complete my dream of studying at a prominent university. I would like to acknowledge my sincerest gratitude toward Asst. Prof. Canras for his continuous efforts in guiding me through the process of research and thesis. His energy and vision kept me motivated all the time. His continuous directional instructions on how to carry out research helped me a lot. His friendship and sense of humor aided me to get through it stress-free.

Moreover, I will thank my parents and my family for their support and understanding and for letting me complete my dream. It takes a lot of courage and fearlessness to send your child to another country. I will also thank my brother Bilal Siddiq as he stood there for me in every problem and took care of both my parents very immensely. My fiancé for her enormous moral support in these 2.5 years. My little sister and nephew Abdul Wali keeping me happy with their presence and make me believe in trusting myself. They all made me capable through their encouragement and backing.

I would especially like to thank Muhammad Inam and Muhammad Haseeb. They are the ones whom I met first when I joined METU. Since then they become more like brothers to me. They guide me and support me always in my academics or in my daily life. They always motivate me to dream big and aim high for my life goals and career. They made my 2.5 years very easy in this university and this friendship will remain last forever like this

Lastly, it will be unjust to not thank my friends here at METU. Each one of them Moaz Zia, Syed Ali, Ahmed Zarar, Mesum Raza, Haider Tasawur Kiyani, Haroon Rasheed, Waqar Orakzai made me feel at home. It felt like home away from home. Through my sickness and busy schedules, they all took care of me like their own brother. They made this whole experience worth it.

TABLE OF CONTENTS

LIST OF TABLES

TABLES

LIST OF FIGURES

FIGURES

LIST OF ABBREVIATIONS

ABBREVIATIONS

(DES) distributed energy resources

(GHG) greenhouse gases

(ESS) energy storage system

(LCOE) Localized Cost of Energy

(MPPT) Maximum Power Point Tracking (MPPT),

(PV) photovoltaic

(IC) incremental conductance

(P&O) Perth and observe

(PEC) Power electronics converter (PEC)

(t_{stand}) standard time

(t_{solar}) solar time

(L_{std}) time zone

($L_{loc)}$ longitude of the location

($I_{b,n)}$ normal component of the beam irradiation

($I_{b)}$ beam irradiation

(NOCT) normal operating cell temperature

CHAPTER 1

INTRODUCTION

According to the polices decide by the climate sector, globally every country is looking forward to decarbonize there power sector and putting efforts in the reduction of the greenhouse gases (GHG), which reduces it side effects with respect to climate change. Because if the steps could not be taken on the earlier notice so it will be catastrophic for us in upcoming days, for this no of treaties and pacts were signed whose aimed is to reduce the global warming by the means of decarbonatization and shift the generation technology towards the renewable and move on the way to the sustainable forthcoming. After these treaties renewable energy such as solar and wing gaining the hype of all researches and over past decade it has been perceive a steep change in these two particular renewable energy resources.

The problem arises that these renewable energy methods differ from other generation technologies in a number of ways, including They behave and are controlled according to their location, and if their major resource varies, so does their production. For example, if there is a cloudy day so PV might not be sufficient to produce the amount of electricity required by the consumer, and the same goes for the wind system if the wind is enough to drive the wind turbine it will cause a lack of power required in the grid for consumers. Sometimes it also happens that our main electricity grids are confronted with issues such as diminishing fossil fuel supplies, inefficient energy use, high power loss, slow response times due to a lack of developments in power distribution automation, and then the question arises how should we make the system efficient and reliable?

The solution came in 2001 by the organization named Consortium for Electric Reliability Technology Solutions (CERTS), They introduce the concept of a microgrid. A microgrid is a system that allows distributed energy resources (DES) to

be integrated into the main grid and to drive load and can also be controlled work in grid-connected mode or islanding mode. In grid-connected mode energy generated from the renewables can be stored in the energy storage system (ESS) or if the demand from the consumer is high enough which main grid cant handle so, It will drive the load with the main grid to meet the demand and if the fault occurs in the main grid it automatically switches itself into island mode where the DES and ESS will drive the load independently and meet the demand of the consumer. Supercapacitors, batteries, pump hydro are examples of the ESS. In previous days ESS is not the viable solution to be a part of microgrid system because it was too much expensive, but nowadays the ESS technology is evolved and the cost of the system is reduced due to which the Localized Cost of Energy (LCOE) is reduced and makes it suitable for the energy markets.

In the microgrid the integration of the main grid to the renewables, ESS, and controlling of the microgrid whether it should work on the island or grid-connected mode done on the bases of the power converter. Power converters are the most essential part of the microgrid, any type of fault that occurs in the converters can cause the whole system to break down. Although microgrids also have their own technical issues like power imbalance, voltage stability, controls, and protection, these all issues remove on the basis of the power converter, So the reliability of the converter is the most concern thing for the smooth operation of the microgrid.

Different issues come across during power conversion, such as condution losses, switching losses, elctro-thermal stress, temperature fluctuations and fatigue which decrease the relaiblity of converter. Electro-thermal stress and temprtaure fluction can create the over voltage or short circuit in the system. For this electrothermal modelling in the system refers a solution to this problem. Electro thermal is divided in two sub systems, First is power loss model which can measure the conduction and switching loses of the system and this modelled is further coupled with the termal model which could generate the temperature of the converter with repect to that power loss. Recently there are diffecrnt apporcahes has been listed in the literature for modelling of the electro thermal block, which can improve the relaiblity of the system. In contrast the

system which is mainting the temperature by varying the switching frequency with the lookup table based powerloss model coupled with thermal model is more prefferd.

1.1 Motivation

All of the micro-grid operations such as switching, controlling, voltage regulation as per requirement are done on the basis of the power converter. The power converter is a controllable device that is proficient in fast switching and has a huge impact on the integration of renewables to the main grid and consumer load, which tells us how much the reliability of the converter is important for microgrids. The reliability of the converter is basically affected by the switching element present in it. Harsh weathering conditions and operations create the electrothermal stress within these switching elements which result, in fluctuations in the temperature of the power converter. This electrothermal stress can create fatigue issues in the solder joints or bonding wire of the switching element which leads to premature failures.

A solution to this problem is to build the electrothermal model which keeps an eye on the temperature of the device and maintains the temperature of the device by regulating switching frequency with respect to the variations that occur in the renewable output. It will mark a significant step toward a more reliable and efficient power electronics device to be in the Microgrids. For a country like Cyprus, which has a lot of solar potential, the idea of implementing the electrothermal model in the power converter can help a lot for a smooth Microgrid operation and will reduce energy crises without having a negative impact on the environment.

1.2 Objective of Study

The main objective of this study is to model a PV-based converter with the electrothermal model, which observes the temperature issues of the switching element of the converter. According to our campus at Kalkanli, Northern Cyprus, the PV is

analytically modeled on excel first and with respect to excel, it is implemented in MATLAB.

There is much research literature is currently available for making an electrothermal model which maintains the temperature of the system by varying the frequency. However, they usually don't have the feature that if the frequency becomes unstable or changes drastically how it can maintain the temperature of the system. The objective of the thesis is to design a PV based converter with the subsystem of Maximum Power Point Tracking (MPPT), electrothermal and lookup table for a variable inductor that responds and maintains the temperature of the system by means of switching frequency on account of weather conditions also if the weather doesn't change and by any means the frequency varies the variable inductor of the converter regulates itself accordingly to maintain the temperature.

The thesis consists of four chapters in which chapter 2 will cover a literature review, which comprehends all areas regarding, MPPT and enhancing the reliability of the converter by using an electrothermal model. The Theory and Methodology used to develop the system will be covered in Chapter 3. The outcomes and examination will be presented in Chapter 4, and the study will be concluded in Chapter 5

CHAPTER 2

LITERATURE REVIEW

Litrerature will be presented in this section with respect to the research which has to be conduct. The study of the relaiblity of the power electronics converter used in renewable energy technology is the key topic in which the cutting edge research is going through out the world to generate the electricity by reducing carbon footprints and to create pollution free enviroment. This literature review which is presented is mainlay focused on the power electronics devices use in renewable energy technology, their failure modes and issues related to relaiblity aspects. Because due to harsh operating condition the temperature issues occur which decreses the lime time of the power electronic device.

On the other hand the solutions and the models have been disscued which integrate in to the system to reduce the temperature which include the power loss model and the electro thermal model. Previous studies for these models will be presented with the comparsion of our proposed model which cater the temperature issue and increase the relaiblity of the power electronic devices used in renewable energy technonlgy.

2.1 Power Electronic Device Used in Solar Energy System

Solar systems are the systems which uses the energy of the sun to power up itself, which uses photovoltaic (PV) cells or PV module to generate the electricity. Solar electricity is an excellent choice because it is one of the cleanest and most cost-effective energy sources available among all renewable energy sources. These are the reasons why solar energy generation and research are gaining traction every day, and investment in the solar sector is fast increasing around the world[1].

First, PV modules generate the electricity which further pass through from DC-DC converter to drive the DC load or if the system is connected to the grid so it uses DC-AC inverter to integrate itself to the utility grid[2]. The maximum power generation of the system depend on the maximum power point tracking (MPPT) methodology, which provide us the control specification at different operating conditions. Those operating parameters use to update in DC-DC converter, which results in to achieve the maximum power form the PV[3].

MPPT depend upon the weather conditions such as temperature and the irradiance of the sun, because the change in the weather conditions can cause the change the maximum power point with respect to I-V cure of the system. Figure 2.1 shows the variations in the irradiance and MPPT accordingly.

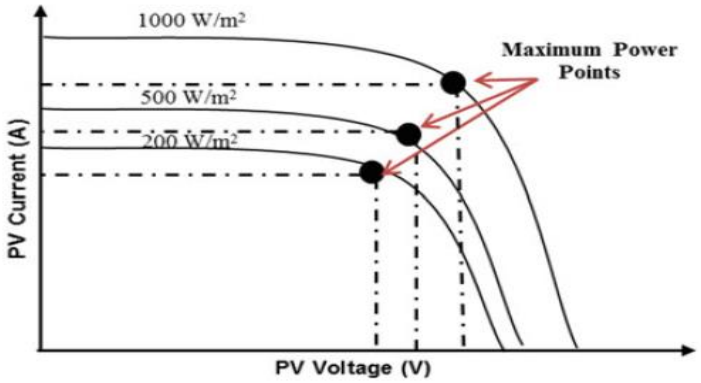

Figure 1 Variation to MPPT caused by Varition of Irridiance

There are two best known methods which are used commonly to extract maximum power known as incremental conductance (IC) and perturb and observe (P&O)[4]. These method uses variations in the switching forms to achieve the maximum power outputs. But in this research the methods are not viable due to its characteristic of working on a fixed frequency. New method for MPPT has been proposed in the methodology section to extract maximum power at variable frequency.

Power electronics converter (PEC) in PV application are the key element, failure in PEC can cause whole system to be broke down. So the reliability of the PEC is most

concern aspect which we have to take in to the account while designing of the system[5]. It has been observe in past several years that in the solar systems PEC inside circuitry has the highest rate of failure among the other devices which around 37% to 40% as shown in figure 2.2[6]. The in-depth understanding of component and system failure progressions is essential to attain reliability, low operational/maintenance costs, and enhanced performance for power electronic converters[7].

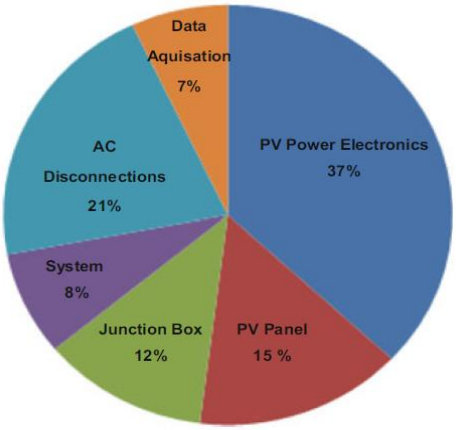

Figure 2 Rate of failure for PV system

To cater these hardware issues of the internal circuitry, physics of failure comes out to be methods which deals with the stress and the defects on power electronics device[8].

2.2 Types of Failure Occur in Power Electronic Device

PEC consists of many electronic components but IGBT is the most vital compenent of the PEC which used intended for switching purpose. Any of the components can be a reason for failure in the system, but IGBT comparatively has high rate of failure among all[9]. The reason behind the IGBT failure is thermomechanical strees, which includes rise in temperature profile and continuous change in operating conditions with respect to PV generation. The structure of the IGBT is composed with several

layers, and these layers are different from each other with respect to material properties as shown in figure 2.3.

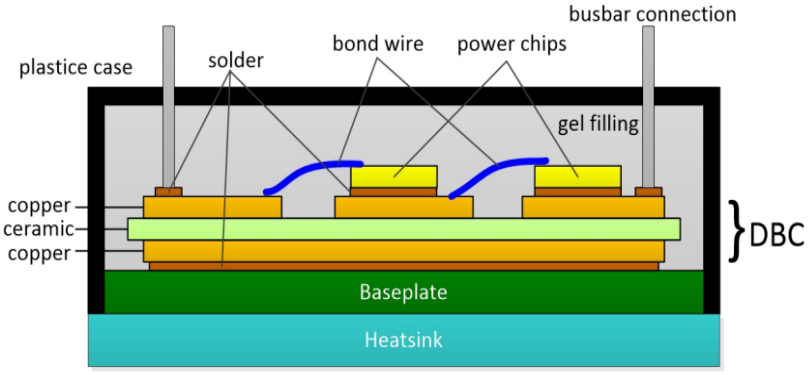

Figure 3 IGBT Structure [10]

When the IGBT is in the operating mode, different heat paths leads heat flux to transfer inside the layers of chip. Due to this thermal cycling, the tempratures varies inside these layers which cause stress in it. Every layer has its pre define co effecients of thermal expansions but the stress due fluction in temperature exceeds these limit, which causes fatigue issues with in the device at several locations and leads system towards the failure. Temperature cycling not only cause fatigue issues but it also create some other stresses which are listed in table 2.1.

Table 2.1 IGBT Failure modes[3]

Failure mechanisms	Failure sites	Relevant loads
Fatigue	Die attach, wire bond/TAB, solderleads, bondpads, interfaces	ΔT, DT/dt, dwelltime, ΔH, ΔV
Corrosion	Metallisation	M, ΔV, T

Electro migration	Metallisation	T, J
Conductive filament formation	Between metallisation	M, ΔV
Stress driven diffusion voiding	Metal traces	S, T
Dielectric breakdown	Dielectric layers	V, T

Where, T temperature, H humidity, D cyclic range, V voltage; M moisture; J current density;Sstress.

Failure of Capacitor in the PECs can also cause voltage stress to the switching dvice and other possible faults which may effects the operations of the whole systems. Capacitors also have there own failure mechanism which has the huge impact to relaiblity of the PECs. Three types of capacitor has been use in the system, metallized polypropylene film capacitors (MPPFC) and aluminum electrolytic capacitors (ALEC) are used as DC link capacitor. When the PV system is integrating in to the grid system and in DC-DC PECs mostly multilayer ceramic capacitors (MLCC) are used[11]. All three has there own failure modes which is listed in table 2.2.

Table 2.2 Capacitor Failure modes[6]

Capactior Type	ALEC	MPPFC	MLCC
Dominant failure modes	Wear out Open circuit	Open circuit	Open circuit
Dominant failure mechanisms	Electrolyte, vaporization; thermomechanical reaction	Moisture corrosion; dielectric loss	Insulation degradation; flex cracking
Most critical stressors	T, V, I	T, V, humidity	T,V, vibration
Self-heating capability	Moderate	Good	No

Addition of a resistor in series with the capacitor commonly known as effective series resistance (ESR) proposed in[12] to make the capacitor relabile for the system.

As compare to capacitors and other electronic components, inductors has minimum rate of failure which is about 3%. The failure in the inductors occur when there is a contionusly change in the inductance and due to overheating[13].

Overall it has been observed that in PECs, IGBT is the most concerd device with respect to relaiblity. In the fatigue issues, particulary bond wire liftoff and solder fatigue are two main failure mechanisum which degrades the life time of the IGBT.

2.2.1 Effects of Wire Bond liftoff

Wire bond liftoff fatigue cause by the aluminium metallization reconstruction which generally increase the on state voltage with in the device. This increment in collecter to emitter voltage increses the themprature fluctuation and power dissipation in the device which results in the form of thermal expansion between the chip and wire bond[14]. Hence, due to this thermal stress wire bond lift off which can be seen in figure 2.4.

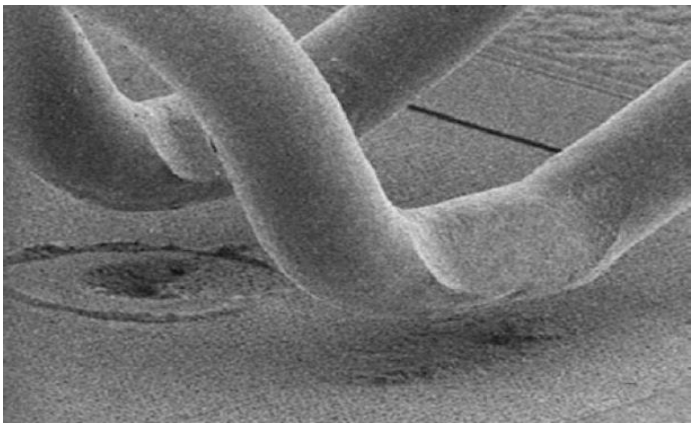

Figure 4 Closed view of wire bond liftoff[15]

When the wire liftoff the device unable to draw the current due to which the load transfer to the other bond wires to conduct more current. Due to which liftoff of the other bond wires occurs continuously because after each liffoff, the current capacity is exceeding the limit[14].

2.2.2 Effects of Solder Fatigue

Solder fatigue means the joints of the solder joints get deform and cracks occurs in it which caused by the temperature fluctuations as shown in figure 2.5 and affects the relability of solder paths.

Differences in thermal expansion characteristics of solder junction layers such as silicon and copper cause such failure. When the stress appear on these layers and the layers mismatched with each other with respect to coefficient of thermal expansion (CTE) causes fatigue[16].

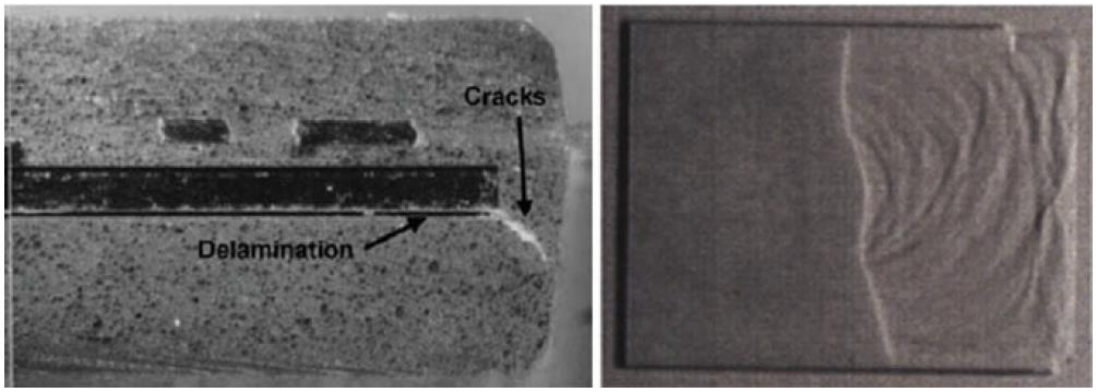

Figure 5 Cracks and solder fatigue[12]

2.3 Review for Power Losses and its Modeling

IGBT and diodes are the primary device for the operation of the converters and while operating, power loss has been occur within these device. So while designing the converter we have to take power loss calculation in to the account[17].

Power losses are divided in two types namely, switching losses and conduction losses. When the device is in transition state from ON to OFF or vice versa, the power dissipated in between this transition is known as switching losses. On the other hand when the device is full conduction mode, the power dissipated while conduction known as conduction current.

Evaluation for the losses of power electronics device can be done from one of the following methodologies which are listed below[18]:

- First method consist of the experimental setup, In which we can not analyze the lossess at every step. From this validation method we just analyze the total power converter loss.
- Second method consist of the physics-based simulations, which uses finite element modelling in which analysis of the IGBT switch can be done in detail. Although the resalts obtain from thses simulation are quite accurate as we compare it with the experimental ones, the problem arises that these simulations are done in an open-loop and our system consist of closed-loop. So, it is impossible to use this methodology for the analysis of the power losses of a closed-loop.
- Third method cosist of behavior modelling. In which the simulation depend upon the parameters for the switching device give by the manufacturer in the form of datasheet. These model with respect to datasheet provide us good results for the analysis of losses but it less accurate as compare to physics-based model. The big advantage of this model is that, we can analyze the losses at each step while designing or If we want total losses it can also provide that. These types of model can also be used in the other simulation tools to simulate the converters with good accuracy results.
- Fourth method consist of the analytical based models also called mathematical models. These models computes very fast and a result, they may be easily integrated in the simulation tools. The results obtain from these

dosent have good accuracy because of there limited operating range in term of voltage and current.

The above listed methodology has been adopted by many of the researcher around the globe. Bilnov et al.[19] propsed the study for analyzing the power losses in which, comparsion has been made for behaviroual and analytical model. Improvement has been made in losses calculation by taking the data from the datasheet provided by the manufacturer. The data has been extracted from the datasheet by using curve fitting method in which losess were obtain by taking current and voltage characterstics in to the account. This data has been compared with the analytical equation drived with respect to the components of the system. The results of this approximation have quite good accuracy but it didn't support in high frequency systems. Similar research was conducted by the Rui et al.[20] in which he made some amendment by including the on time resistance and the temperature loses in the calculation of power losses and highlight the importance for this in his estimations. The simulation for this model has been carried out in the software named PSCAD and it was proved from the results that after incluing this loses, the accuracy for the model is increased and the error comes out be around 1.4% with respect to analytical model. This error percentage is quite low as compare to the previous research. However Ivakhno et al.[21] adopted the similar approach but the executaion of the model done on the different software named MATLAB/SIMULINK[22]. The logics block were used to implement the power loss equation, which dependend upon the output of IGBT and diode in the form of current and voltage signals. The accuracy under this methodology is acceptable which about less than 10%.

With in the aspect for relaiblity analysis, electrothermal modelling has a great impact on it beacuase involving the electrothermal model would increase the accuracy of the power losses analyses. Zhou et al.[23] proposed this method for integration electrothermal model in the power model for the accuracy, In which the simulations were done on the bases of lookup table.

Hence it has been obsereved that the importance of the power model is increasing nowadays, and through out the globe still the work is going on in this field to built , fast , accurate and simple power loss calculation methods.

2.4 Review for Thermal Modelling

Switching devices which are used in PEC and it application such as, electric vehicle, microgrids, smart grids, motors drives, gets heat up and generate thermo-mechanical stress due to power dissipation. The breakdown of the switching device due to this thermo-mechincal stress is the main cause for the failure of the power converter. To cater this issue there is need for the thermal model which use to keep an eye on the temperature of the switching device at harsh operating conditions, so that solution should be provide to maintain the temperature of the device before it breakdowns[24],[25]–[28].

In order to make the accurate thermal model many study has been proposed, some them rely on physics based simulation and some them are based on electrical parameters. Finite element Modelling is the most renowed physics based simulator which is used to conduct the simulations for heat transfer with in the device. The problems arises that there computational time is very long and it cannot be integrated to electrical based simulations of the converter[24].

So electrical based thermal models are the best fit for the thermal anlysis of the switching device. These thermal models are known as RC thermal network based on the RC equivalent circuits, which represents the device thermal characterstics[29]. There are two types of RC thermal networks namely, foster and cauer models as shown in figure 2.6 and 2.7.

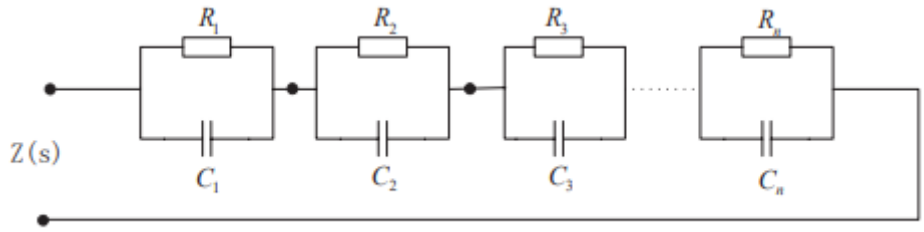

Figure 6 Foster Model[21]

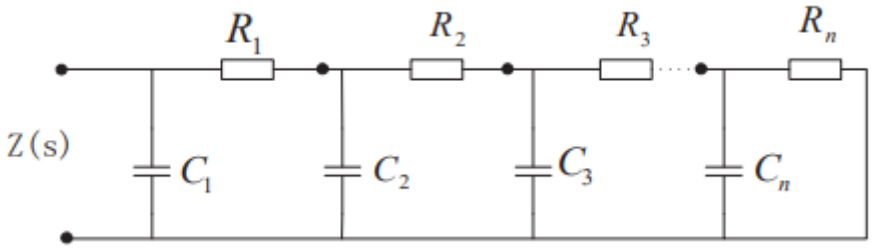

Figure 7 Cauer Model[21]

The above shown RC thermal models are similar to the heat conduction models in one dimension and with respect to the electric thermal theory the voltage of the circuit is use to define the junction temperature. However the thermal resistance and heat capcity is defined by the circuits resistanace and capacitance.

The cauer model shows an accurate representation and thermal behvaiour of the device because it depent upon the physical structure and parameters of the switching device. It can represent the thermal behavior of the each internal layer of the device[30], [31]. On contrast with the foster type RC model, which is most widely use method due to its independency form the internal structure of the device. It depends upon the system parameters and directly generate the junction temperature for the whole device instead of each layer. Many significant studies and research reports are reported to measure the device thermal performance using thermal equvivalent circuits[32].

Yalcin et al[33] consuct the research in which he stated that, depending upon the the thermal resistance provided by the manufacturer in the data sheet can lead to the

many significant errors. He adopt the curve fitting method by use excel macro to extract the value of RC network form the thermal impedance curve. This methodology can be taken as the most simplest way of generating thermal model for switching device, but is only useful where only the junction temperature of the device is going to be studied. The cauer thermal model which takes into the account, the temperature affects on to the thermcal conductivity is proposed by Chuyu Tian et al[29]. In which the model validation has been done by comparing the calculated junction temperature with the output of the simulations performed at COMSOL mutli-physics based software. This study can bbe utilized where the physical structure (layers) of the device taken in to the account. The modification in foster thermal model on the bases of number of network ladders was proposed Ali Akbar et al[34]. In which the model predicts the transient behavior with respect to non linear system and according to the simulation the accuracy of the result was high and error is calculated about 5%. In which it is proved to get the good accuracy, high number of the ladders is required.

The progressive Foster thermal model which is based on the frequency domain is proposed by Ke Ma et al[35]. In which he mentioned the limits of the previous RC based models with respect to the frequency domain and proposed the new model. This model can be easily determined by defining the slope deviation from the commonly used Foster thermal bode plot. It can not only predict the temperature of the device but it can also identify the heat streaming out from the device. In the comparsion with the current models, it predicts the more accurate temperature of the device.

Recently the auspicious study is done by Xianrong Fan et al[36] in which effect of different parameter on the device junction temperature is diccussed. The proposed model is based on the foster type model with electro-thermal coupling technique in which RC components are extracted from the thermal impedance cure by using the tool box name fitting in the matlab, which is based on curve fitting method. This model not only calculate the loss and junction temperature but also reflect the change

in the temperature due to change in system parameters, such as change in period of current lead to the change in transient behaviour of temperature of IGBT module.

The similar work was proposed by the Canras et al[37] with high accuracy as compared to previous study. So in this thesis research the parameters of the thermal model has been adopted form that research article.

2.5 Gaps in Literature

Some of the following research gaps are found after the intensive literature review with respect to the powers loss and thermal modelling of the switching device and their importance towards the relaiblity of the system.:

1) According to the literature there are many power loss and electro-thermal model has been proposed but on constant system parameters no work has been published while encoutring the affects after changing the systems parameters.
2) The MPPTs present in the literature for PV system all worked with respect to constant frequency, no proper study has been available regarding MPPT which worked on variable frequency as in the system we have to maintain the temperature by varying the frequency.
3) The proper literature is not available for designing the controls for the system which vary the frequency and the inductor value at the same time with respect to ambient temperature, However at the same time achieve the MPPT for that system.

The main reason for to do the research in this topic is that, METU NCC has 1 MW PV plant running in the university which faces the issue regarding the failure of the power converters due to harsh operating conditions. So this study is done according to future prespective to increase the relaiblity of the converters while encountering its temperature issues.

CHAPTER 3

THEORY AND METHODOLOGY

3.1 Data

The data which we are using for modeling the PV is the data of our campus (METU -NCC). This data is collected from the solar farm of our campus by using sensors. Data is comprised of the hourly irradiation level of the farm for 365 days. Simulation can be done by using the data for one day at a time. Matlab has been used to simulate the data for June 23rd [38], because data shows that this particular day has the highest irradiance level and it is considered to be the longest day for that year. So it can be observed that after applying switching algorithm how much we reduce the temperature of the converters it self to make it reliable.

3.2 Model

The PV system with a DC-DC power converter has been designed in this study. The array module of the PV is connected to the power converter for boosting the voltage up to requirement. The voltage output of the PV panel is controlled the by Maximum power point Algorithm (MPPT). In this, a study we have designed our own MPPT which can work on the variable frequency. The converter contains the lookup table for the inductor values, so the inductor varies itself with respect to the duty cycle and frequency. This model also contains a power loss and thermal model which use to calculate the power losses and with respect to that loss the change in temperature can be detected of the device. This thermal model helps us to keep an eye on the temperature fluctuations so that we can reduce them by using a variable switching

algorithm and enhance the reliability of the converter. Flow chart and the simulink model of the system can be seen from the figures below.

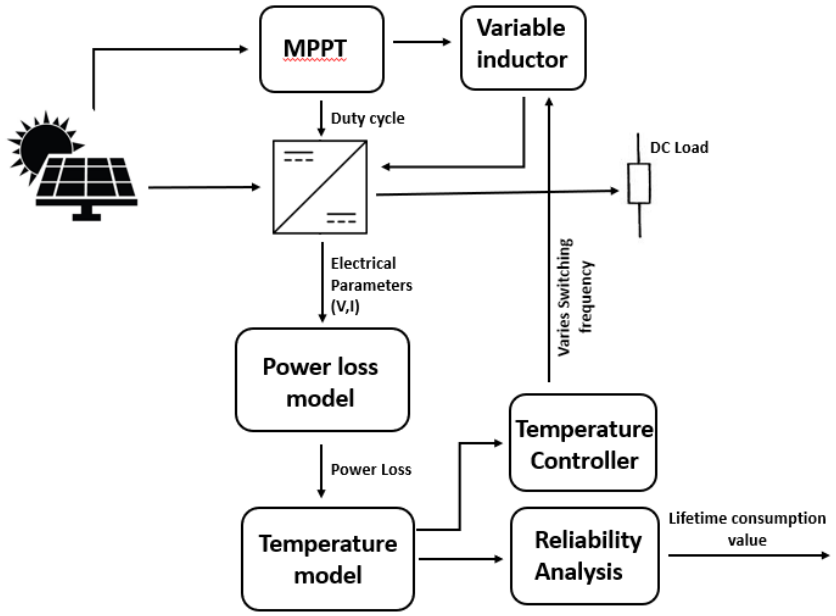

Figure 8 Flow chart of PV based system

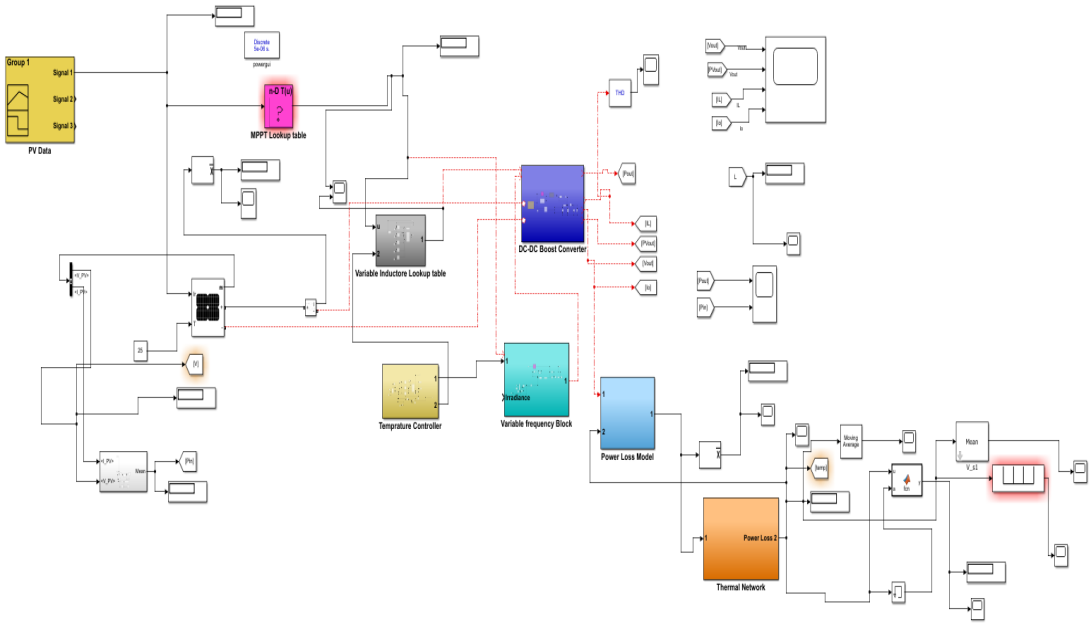

Figure 9 Simulink Model

3.3 PV modeling

The solar radiations hit the PV differently with respect to the location of the earth, because earth use to rotate around the sun to its axis. This is the reason that world has been divided into different time zone. So, for the different locations and with respect to these locations comparison of the tilt angle can only be done after standardizing the time.

To obtain the tilt angle our first step is to convert the standard time (t_{stand}) in to the solar time (t_{solar}), because solar time identifies the the location of the sun on the sky. For the solar time calculation, the time zone L_{std} , the longitude L_{loc} of the location and the equation of time E are taken in to the account. This time equation can be found with respect to specific day number of each month. These below equations 3.1, 3.2, 3.3 are used to find the solar time and the equation of time[39].

$$B = (n-1)360/365 \tag{3.1}$$

$$\begin{aligned} E = 229.2(0.0000075 + 0.001868\cos(B \\ - 0.032077\sin(B) - 0.014615\cos(2B) \\ - 0.04089\sin(2B)\ ) \end{aligned} \tag{3.2}$$

$$t\_s = t\_std + (4(L\_std - L\_loc\ ) + E)/60 \tag{3.3}$$

The relation between the position of the sun and any of its position from the Earth or ground can be identify by using solar time equation, Due to which the tilt angle which is obtain at different locations can be standardize. As the earth rotation per hour is about 15° and the conversion of the solar time to the angle which is known as hour angle *ω, has* to be taken in to consideration while using the values solar time in our calculations. It provide us positive values for the afternoon and the negative values for the mornings, which is calculated by the given equation 3.4[39].

$$\omega = (t\_s - 12) \times 15 \tag{3.4}$$

The Latitude φ is another variable that varies accordingly on the bases of location. The angular position of a location with relation to the equator is represented by latitude. The earth use to rotate around the sun at fixed axis,

Another parameter which changes depending on the location is the Latitude φ. Latitude represents the angular position of a location North or South with respect to the equator,

However there is a little tilt in the axes due to which the suns angular position changes and instead of being constant. As a result while computing tilt this also has to be take in to consideration. For this purpose Decimation angle δ has been used. It depicts the Sun's angular position in relation to the equator at midday. Equation 3.5 is used to calculate it[39].

$$\delta = 23.45 \sin(360((284 + n)/365)) \quad (3.5)$$

Additional parameter which is dependent on location and taken into account is surface azimuth angle γ. It is use to represent the angle of projection normal to the surface and South, and which is lie between -180° to +180° range. Its value is positive for West of South and negative for East of South.

By using the variables listed above, now the tilt angle can be determined. The solar altitude angle α_s and the zenith angle θ_z are determined first. Zeinth angle shows the relationship between beam radiation and vertical (normal to the horizontal) which can be calculated by using the equation 3.6[39].

$$\cos(\theta\_z) = \cos(\phi)\ \cos(\delta)\ \cos(\omega) + \sin(\phi)\ \sin(\delta) \quad (3.6)$$

The accompaniment of the zenith angle is solar altitude. The angle between the projection of the radiation on the surface which is horizontal and South is azimuth angle γ_s . zenith angle, hour angle , declination angle and the latitude angle are the

parameters on which it is dependent, and can be calculated from the equation 3.7, 3.8 and 3.9[40].

$$sign(\omega) = \begin{cases} -1, & \omega < 0 \\ 1, & \omega \geq 0 \end{cases} \tag{3.7}$$

$$\gamma_s' = \begin{cases} \dfrac{\cos(\theta_z)\sin(\phi) - \sin(\delta)}{\sin(\theta_z)\cos(\phi)}, & \theta_z \neq 0 \\ 1, & \theta_z = 0 \end{cases} \tag{3.8}$$

$$\gamma_s = \begin{cases} sign(\omega)|\cos^{-1}(\gamma_s')|, & \gamma_s' \neq 1 \\ 0, & \gamma_s' = 1 \end{cases} \tag{3.9}$$

The angle of incidence θ can now be calculated. Tracking with respect to three different schemes are used for it. First is done without any involvement of tracking, which is between the angle of beam radiation with respect to surface normal and surface. Equation 3.10 is used for its calculation[39].

$$\cos(\theta) = \cos(\theta\_z)\ \cos(\beta) + \sin(\theta\_z)\ \sin(\beta)\ \cos(\gamma\_ - \gamma) \tag{3.10}$$

E-W tracking for the single axis and the angle of incidence for this can be calculated by using equation 3.11[39].

$$\cos(\theta) = [1 - \cos\text{^}2(\delta) \quad \llbracket \sin\text{^}2(\omega) \rrbracket]\text{^}(1/2) \tag{3.11}$$

Tracking for the 2-axis and the angle of incident for that will always be identical as the panels were being adjusted for real time, in which the surface is always perpendicular to the incidence of the beam radiation.

The irradiation data and the relations for solar geometric can be used to calculate the energy generation. For this extraterrestrial normal insolation $I_{o,n}$ is required, which can be defined as the normal unaffected solar radiation by the atmosphere of the Earth. Equation 3.12[38] can be used to calculate it, the equation also contain G_{sc} which is the constant known as Solar contact (G_{sc} = 1367 W/m$^{2.}$).

$$I\_(o,n) = G\_sc\ (1 + 0.033 \cos\ (360/365\ n)\ ) \quad (3.12)$$

Now the extraterrestrial irradiation I_o can be calculated by evaluating the extraterrestrial normal irradiation in equation 3.1[39].

$$I\_o = I\_(o,n)\ \cos\ (\theta\_z\ ) \quad (3.13)$$

From the DNI data provided in the TMY dataset and the extraterrestrial irradiation, we can calculate the clearance index $k_{T,}$ it tells us about the distribution of the frequency with respect to cloud cover which is always in range from 0 to 1. It can be calculated by using equation 3.14 [39].

$$k\_T = I/I\_o \quad (3.14)$$

With the above parameter we can now find horizontal diffusion irradiation I_d. Orgil and Holland's correlation defines the relation between horizontal diffusion irradiation and clearance index, and can be seen in below equation 3.15[39].

$$\frac{I_d}{I} = \begin{cases} 1 - 0.294k_T & k_T < 0.35 \\ 1.577 - 1.84k_T & 0.35 < k_T < 0.75 \\ 0.177 & k_T > 0.75 \end{cases} \quad (3.15)$$

Now we can find out the beam irradiation I_b by using the above parameter named as diffuse irradiation. Three type of irradiation can be used to determine the horizontal global irradiation namely, beam, reflected and diffuse irradiation. Reflected irradiation has been neglected in this research work and now beam irradiation can be calculated by using equation 3.16[39].

$$I\_b = I - I\_d \quad (3.16)$$

Now the normal component of the beam irradiation $I_{b,n}$ can be calculated with respect to beam irradiation $I_{b.}$ The incidence on the surface is represented by this normal component of irradiation and can be calculated by using equation 3.17 [39].

$$I\_(b,n) = I\_b/\cos\ (\theta\_z\ ) \quad (3.17)$$

As we know the we have to tilt the PV panels at some angle to achieve the maximum power generation due to tilt angle there is a change in component of beam irradiation and diffuse irradiation and it can be obtain by using equation 3.18 and 3.19[39].

$$I\_(b,T) = I\_(b,n)\ \cos(\theta) \quad (3.18)$$

$$I\_(d,T) = (I\_d\ (\cos(\beta) + 1))/2 \quad (3.19)$$

PV modules are not only depend upon the irradiance for energy generation but it also depend upon the type of the PV panels which is used. Because there are several factors which can affect the energy production such as normal operating cell temperature (NOCT), it is the temperature of the solar cell on which it is tested at nominal irradiance, irradiance, temperature coefficient, PV efficiency at ambient temperature, and reference efficiency. The PV module used is 250 W manufactured by the Axitech, whose specifications are given in the Table 3.1.

Table 3.1 Specifications of Axitech 250 W PV Panel

Parameter	Symbol	Value
Reference Efficiency	$\eta_{PV,ref}$	0.1537
Area of PV Module	A (m^2)	1.63
Rated Power	P (W)	250
Irradiance at Standard Test Conditions	G_{STC} (W/m^2)	1000
Temperature at Standard Test Conditions	T_{STC} (^oC)	25
Nominal Operating Cell Temperature	NOCT (^oC)	45
Irradiance at Nominal Operating Cell Temperature	$G_{ref,\ NOCT}$ (W/m^2)	800
Temperature at Nominal Operating Cell Temperature	$T_{ref,\ NOCT}$ (^oC)	20
Temperature Coefficient	β_{ref} (1/K)	0.0042

In the table above the efficiency which is mentioned is for the standard test condition.

When on the PV module the solar irradiance incidences, the temperature of the cell increases due to which the efficiency of the module also changes, this change can be calculated by using equation 3.20[39].

$$T\_cell = T\_amb + (NOCT - T\_(ref, NOCT)\ )I/G\_ref \quad (3.20)$$

After the cell temperature has been determine, by using this temperature new efficiency can be calculated by using equation 3.21[39].

$$\eta\_PV = \eta\_(PV, ref)\ (1 - \beta\_ref\ (T\_cell - T\_STC\ )) \quad (3.21)$$

The amount of the power produce by the single module can be obtain by using equation 3.22[39].

$$I\_PV = \eta\_PV\ I\_T \quad (3.22)$$

Now finally the amount of the energy produce by the whole plant can be obtain by using equation 3.23[39].

$$E\_gen = I\_PV \times A \times Number\ of\ Modules \quad (3.23)$$

3.4 PV control modeling

As we know that the output of the PV module is depend on the irradiance and the irrdiance varies with respect to weather and the day light due to which the PV output also varies. The aim is to regulate the power supply in such manner that we will generate maximum power. In order to fulfill our requirement, we use boost converter in our research and the gate pulse applied to switch (IGBT) of the converter in way a that, we achieve the maximum power output from PV.

All the previous algorithms to achieve maximum power such as Incremental Conductance Method (ICM) and Perth and Observe Method (P&O). They are failed to provide maximum power in this research because they worked on the fixed

frequency, and our systems worked on the bases of variable frequency to minimize the temperature fluctuations of the converter as discussed above.

So for our model we use lookup table method in which we define the values of the duty cycle at every irradiance and as the irradiance changes the lookup table select the value of duty cycle from the table[41], [42]. The value of duty cycle then goes to the PWM block which generates the pulses accordingly due to which we achieve maximum power at variable frequency too.

First we find out the input and output voltage and current of the PV panel with respect to our load which is 1000 ohms and then with that voltage and current we find out duty cycle by putting the values in boost converter duty cycle equation 3.24.

$$D = 1 - \frac{Vi}{Vo} \tag{3.24}$$

The table for MPPT designed in MATLAB is shown in Table 3.2.

Table 3.2 MPPT duty cycle

Irradiance	Duty Cycle
100	0.470
200	0.494
300	0.500
400	0.510
500	0.514
600	0.518
700	0.521
800	0.524

900	0.527
1000	0.530

3.5 PV Interfacing DC-DC Boost Converter

While extracting energy from the renewables we experience that it has very low voltage output to drive any load due to which DC-DC to converters are required to boost that voltage to the required level. Boost converter is used in that case to boost the voltage. Efficiency, output power is the main concern for the boost converter while designing[43].

The output of the boost converters is controlled by the MPPT block which is discussed in the above section. This on and off duration is represented by "D" known as the duty cycle of the converter by varying the duty cycle our output of the converter also varies.

3.5.1 Conventional Boost Converter

Boost converter is used to step up the input voltage to required value. It is shown in the figure 3.3 below. It is relatively simple configuration where a switch controls the flow of current to obtain a certain voltage output[44].

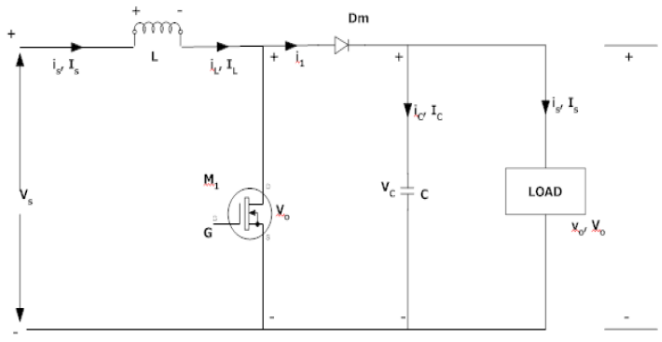

Figure 10 Conventional boost converter schematic

The boost converter has two operational modes when the switch is on and off. In mode 1 the switch is on, and the current will flow through the inductor, storing energy and the capacitor feeds the load. The circuit during ON mode is shown in figure 3.4.

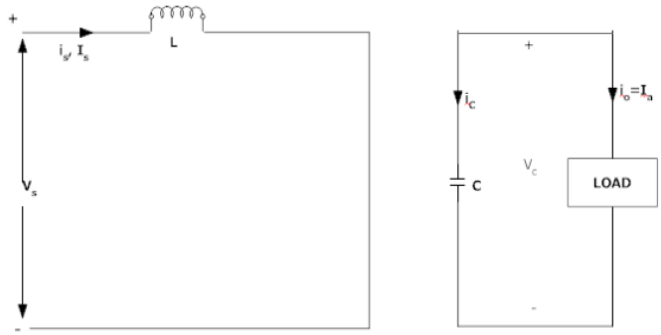

Figure 11 Conventional boost converter at ON stage

In the mode 2 the switch off and the current flows from the inductor, capacitor, and the load. The current of the inductor decreases because the energy stored is now released and flows through the load as shown in the figure 3.5.

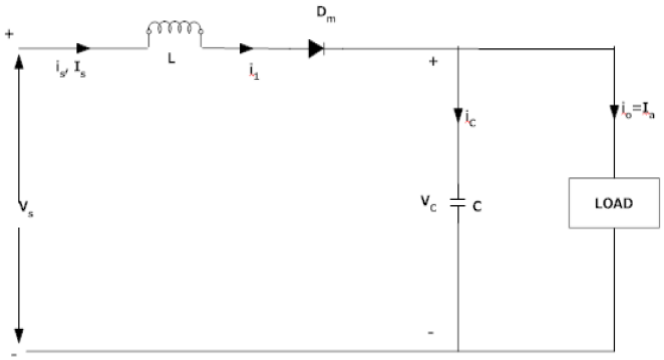

Figure 12 Conventional boost converter at OFF stage

3.5.2 Derivation of Transfer Function

Input to output relation of boost converter can be seen in equations 3.25 and 3.26, it is drive by doing the steady state analysis[44][45].

$$V_d t_{on} + (V_d - V_o) t_{off} = 0 \tag{3.25}$$

Dividing both sides by T_s.

$$\frac{V_d t_{on}}{\mathrm{Ts}} + \frac{(V_d - V_o) t_{off}}{\mathrm{Ts}} = 0$$

$$V_d D + (V_d - V_o)(1 - D) = 0$$

$$\frac{V_o}{V_d} = \frac{1}{1 - D} \tag{3.26}$$

3.5.3 Selection of Design Parameters

There are four different parameters which has to be taken into account while designing the boost converter namely[46]:

1. Semiconductor (switching device)
2. Diode
3. Capacitance
4. Inductance

1) Semiconductor (switching device)

The selection of the switching has to be done with respect to some characteristics, that it has to be strong enough, can face the voltage and current stress in the worst scenarios. This current and voltage can be identified by using equations 3.27 and 3.28 after which we can select the switching element of the converter as per our requirement[44].

$$V_{stress} = V_{PV\,max} \tag{3.27}$$

$$I_{peak} = I_{output} + I_{ripple} \quad (3.28)$$

Where $V_{pv\,max}$ can be defined as the maximum output of the PV module for the boost converter.

2) Diode Selection

The diode has been chosen in a way that it can be capable of handling the average and peak current of the system, blocking the off-state voltage stress, fast switching capability, small forward voltage drops, and less reverse recovery time.

3) Capacitance

The capacitor in the boost converter is also known as the filter capacitor, which is used to reduce the voltage ripple and keep then within the limit of the ripple specification of the system. The value of the capacitor can be determined from equation 3.29 with respect to switching frequency, ripple percentage, and duty cycle[44].

$$C = \frac{Vo*D}{F_s*\Delta Vo*R} \quad (3.29)$$

4) Inductor

Sizing of the Inductor plays a key role in the power efficiency of the system otherwise it can affect the system because in this research we have two parameters (duty cycle, and switching frequency) which are changing with respect to irradiance to keep temperature of the switching element constant. Due to these changing parameters, we face two problems which are listed below:

1. From the above mentioned MPPT table we have observe that in order to achieve the MPPT the duty cycle has been adjust sue to which sometimes the problem occur while changing the duty cycle the converts shifts from continuous conduction mode CCM to discontinuous conduction mode DCM. So, in order to maintain the system work in the loop for continuous conduction mode we have to adjust the value of the inductor with respect to

duty cycle. There relation can be seen from equation 3.30 that duty cycle is directly proportional to inductor size.

2. The current rating of the converter depends upon the ripple percentage of the current. So, it has to be maximum due to which we get smaller inductance. Because decreasing the inductor can cause a higher current for the system. The problem arises with the ripples when the variable switching algorithm respond in the harsh weathering conditions. The algorithms vary the frequency to make the temperature constant at higher frequencies the ripples reduces but when the frequency goes down the systems experience the higher ripples which affects the power efficiency of the system. So, in this case at lower frequency to reduce this power loss, the inductor can be sized for the maximum current. The relation can be seen form the equation 3.30 that switching frequency and the ripples factor is inversely proportional to the inductor value.

So, in this research inductor has been designed by the means of variable. The variable inductor varies it self by at the time of the change in duty cycle and switching frequency so that it will run the system smoothly in CCM and even achieve the power efficiency more by keeping the ripples constant while the frequency is changing. Below equation 3.30 is used to find the values of the inductor[44].

$$L = \frac{V_d * D}{\Delta I * F_s} \qquad (3.30)$$

in which the frequency varies from 1kHz to 20kHz, ripple factor is varies from 2% to 20% and duty cycle varies from 0.3 to 0.7. the values for the inductor are used in the system in the form of lookup table which can be seen in the figure below.

		Ripple %				
		2	5	10	15	20
Frequency kHz	1	10.5	4.2	2.1	1.4	1.05
	5	2.1	0.84	0.42	0.28	0.21
	10	1.05	0.42	0.21	0.14	0.105
	15	0.7	0.28	0.14	0.093333	0.07
	20	0.525	0.21	0.105	0.07	0.0525

Figure 13 Variable Inductor Values for DC 0.3

The tables for other duty cycles are lised in the appendix section and the table below shows the design parameters of the boost converter used in this research.

Table 3.3 Specifications of Boost Converter

Parameter	Unit	Value
Input voltage	V	420
Output voltage	V	870
Rated Power	W	8000
Load	Ω	1000
Low voltage capacitor	F	200µ
High voltage capacitor	F	600µ

3.6 Power Loss Model

During the operation of the IGBT, there are two types of energy losses we experience which are; first one is the switching loss which we calculate in terms of energy loss with respect to the switching of the device over one period of time. This loss is calculated when there is a change in current I_{ce} and voltage V_{ce} at the time of switching either in the conduction state or blocking state due to which this loss has been divided into two parts, switch on and switch off loss represented by E_{on} and

E_{off}. The second one is the power conduction loss which occurs when the IGBT is conducting current and is represented by P_{con}[47].

In this research Individual power loss data for IGBT was used as shown in fig 3-4 and 3-5 provided by the manufacturer of the power electronic device. We put these data into a lookup table so that the lookup table can generate the value of power loss for the device with respect to current, voltage, and junction temperature.

Column	(1)	(2)	(3)	(4)	(5)	(6)
	0	***7.91***	***12.16***	***20.08***	***30***	***50***
25	0	0.036541667	0.050333333	0.080166667	0.112666667	0.202875
50	0	0.03875	0.054541667	0.082083333	0.130208333	0.204458333
80	0	0.043541667	0.058375	0.090541667	0.12725	0.232375
100	0	0.046208333	0.06225	0.095708333	0.147958333	0.238875
125	0	0.051208333	0.067875	0.103458333	0.14375	0.268375

Figure 14 Swicth On Loss Lookup table

Column	(1)	(2)	(3)	(4)	(5)	(6)
	0	***7.91***	***12.16***	***20.08***	***30***	***50***
25	0	0.0493	0.0676	0.0985	0.131	0.2
50	0	0.052333333	0.073041667	0.10325	0.142166667	0.203666667
80	0	0.053458333	0.074125	0.104583333	0.146458333	0.211041667
100	0	0.054666667	0.0745	0.106541667	0.1505	0.213916667
125	0	0.055791667	0.075583333	0.108916667	0.149958333	0.212916667

Figure 15 Swicth Off Loss Lookup table

These losses in the lookup table are estimated analytically by the equations 3.31, 3.32, and 3.33 shown below.

$$E_{sw} = \int_{on} E_{on}\,.(t)dt + \int_{off} E_{off}\,(t).dt = f(V_{ce}, I_{ce}, T_j) \qquad (3.31)$$

Now power loss can be obtained by converting this energy loss into power loss by multiplying the switching frequency with it, which can be shown in the equation below.

$$P_{sw} = (E_{sw}) * f_{sw} \qquad (3.32)$$

The second loss in terms of power is conduction loss represented by P_{con}, and it can be calculated by using the equation shown below.

$$P_{con} = V_{ce} * I_{ce} = f(I_{ce}, T_j, D) \quad (3.33)$$

Where T_j is the junction temperature, V_{ce} is the collector to emitter saturation voltage, I_{ce} is the collector to emitter current and D is the duty cycle of the system. Simulink model for the power loss can be seen in fig 3-6[48].

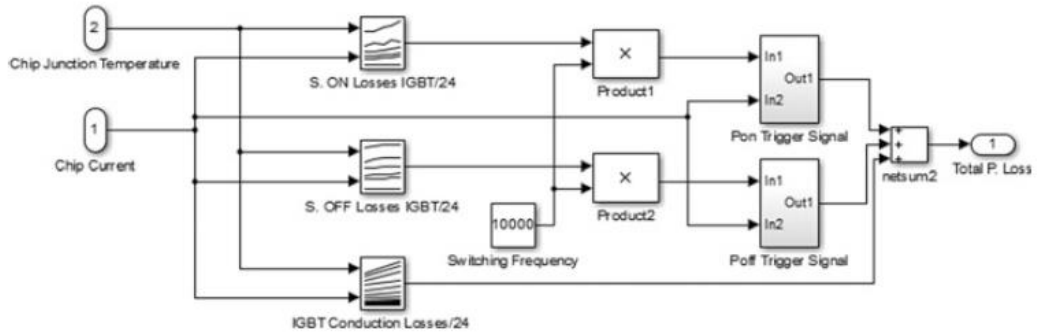

Figure 16 Power Loss Model

3.7 Electro-Thermal Model

To build the thermal model we have to take all the individual layers present inside the semiconductor, we use the transfer function to represent these layers to see the behavior of the semiconductor device with respect to temperature. To represent the transfer function of the layers there are two types of thermal network circuits namely, cauer and foster. These methods consist of RC elements. Each RC element is used to represent the thermal capacitance and resistance of each layer and gives us the equivalent circuit of the switching device, which determines the switching device's actual temperature.

In this research, we use a foster thermal network due to its advantage of containing the physical characteristic of each layer. Foster network is built by the RC element

of each layer connected parallel and further connected into series with parallel combination RC element of other layers as shown in fig 3-7[49].

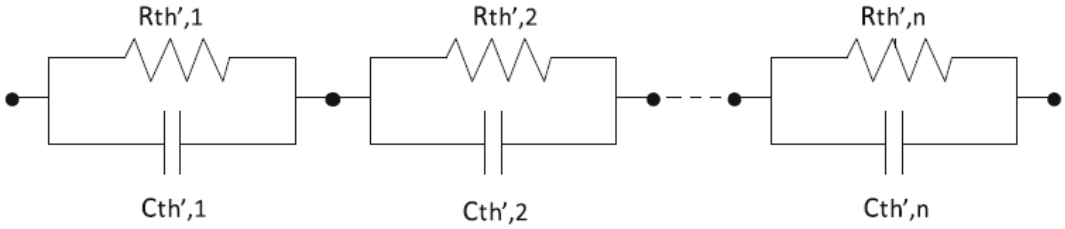

Figure 17 Foster Thermal Network

Transfer function with respect to thermal impedance for each layer can be found by using equations 3.34 and 3.35

$$Z'_{th} = \frac{\frac{R'_{th}}{1}}{sC'_{th}} = \frac{R'_{th}}{sR'_{th} * C'_{th} + 1} \tag{3.34}$$

By rearranging equation 3.34 we get,

$$Z'_{th} = \frac{1/C'_{th}}{s + 1/\tau} \tag{3.35}$$

where,

$$\tau = R_{th} * C_{th}$$

The thermal capacitance C_{th} and R_{th} for thermal block shown in figure 3-8 is taken from [50]which is extracted by using curve fitting least square method.

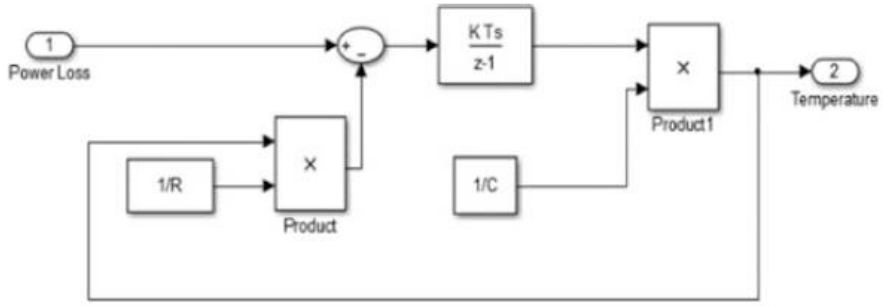

Figure 18 Thermal Network Model in Simulink

Data has been used in the form of lookup table can be seen in figure 3-9 which is used to interpolate the data for predefined R_{th} and C_{th} in the Simulink block of thermal model, so it could generate the temperature of the device.

Device LUT	Thermal Capacitance			Thermal Resistance		
	$C_{th,1}$	$C_{th,2}$	$C_{th,3}$	$R_{th,1}$	$R_{th,2}$	$R_{th,3}$
IGBT	0.134	0.294	26.89	0.343	0.329	0.322

Figure 19 Lookup table for thermal Network

CHAPTER 4

RESULTS AND DISSCUSSION

Results and disscussion section is divided in to four subsection. In first two section validation off the experimental values of conventinal boost converter has been done with respect to simulated values of the same conventional boost coverter simulated in Matlab Simulink. In other two section advancement has been made in the previously defined PV- based DC-DC converter to make the temperature profile constant at harsh weathering condition so that reliability of the converters increased.

4.1 Temperature Verification for Conventional Boost Converter

Hardware prototype and Simulink model for the conventional boost converter can be seen form the figure below which has built in order to verify the temperature profile.

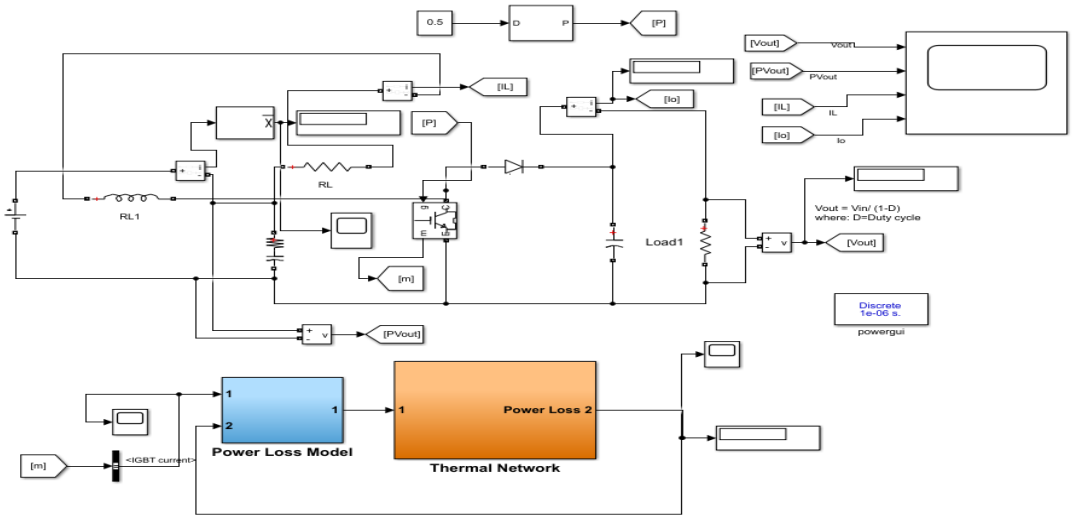

Figure 20 Simulink model for boost converter

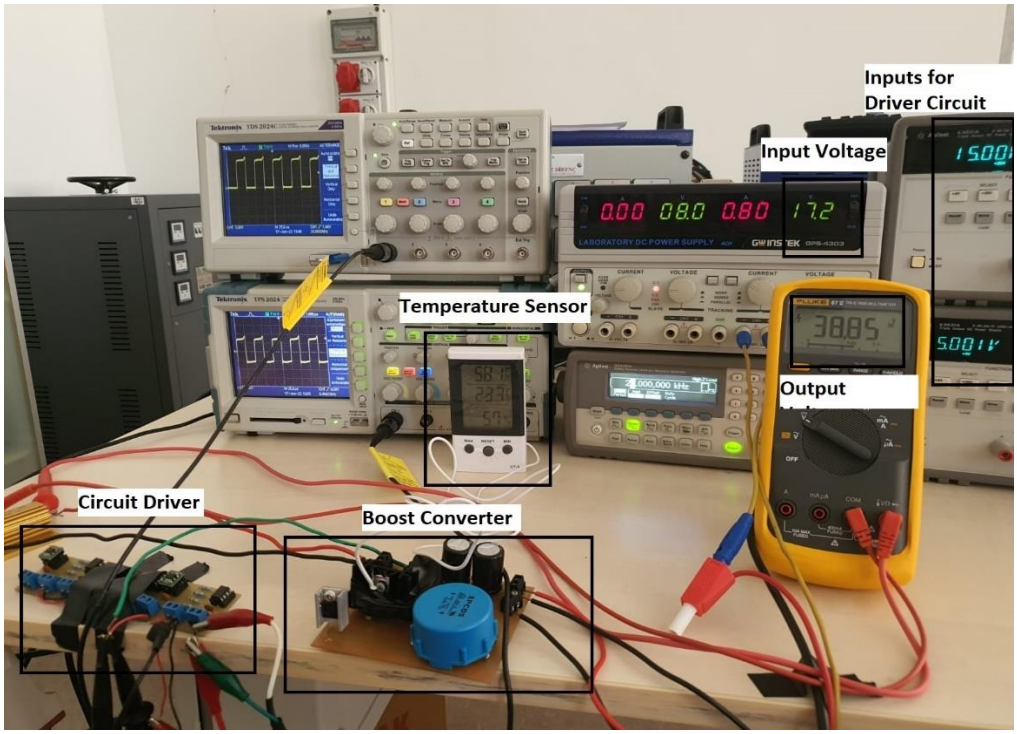

Figure 21 Experimental Setup

4.1.1 Temperature Verification with Different Switching Frequencies

In order to verify the temperature profile of the switching element with three different frequencies (10 kHz, 15kHz and 20kHz) while having the input of the system remains constant. Both simulated and experimental results for these frequencies can be seen in figure 4-1, 4-2 and 4-3.

From 4-1, it has been observed that experimental results are verified according to simulations. Experiment results also follows the same trend for temperature with average error of 3% which is quite acceptable with respect to experimental errors. The results are started from the ambient temperature of 25°C and after 10s the temperature of the switching element for both the results can be seen around 50°C.

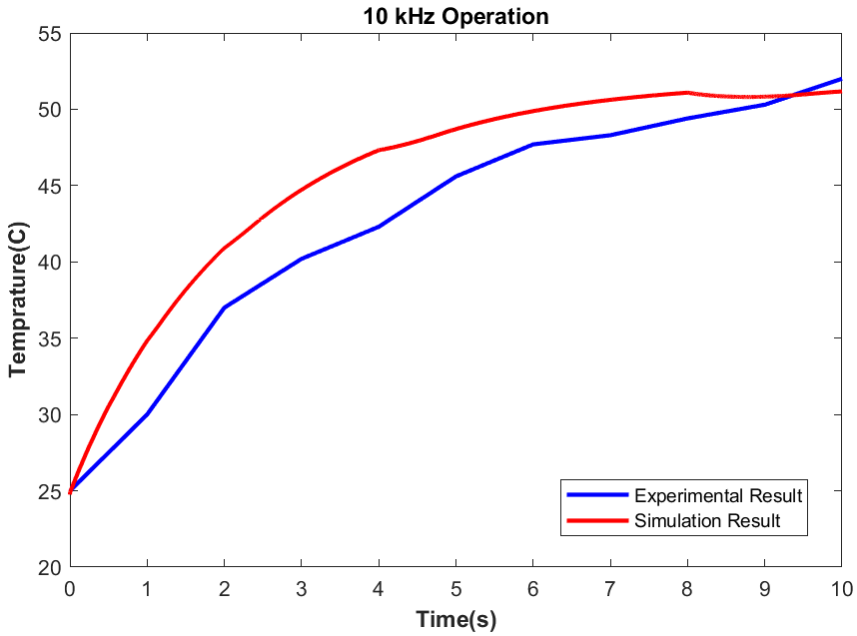

Figure 22 Switching Element Temperature Graph at 10kHz

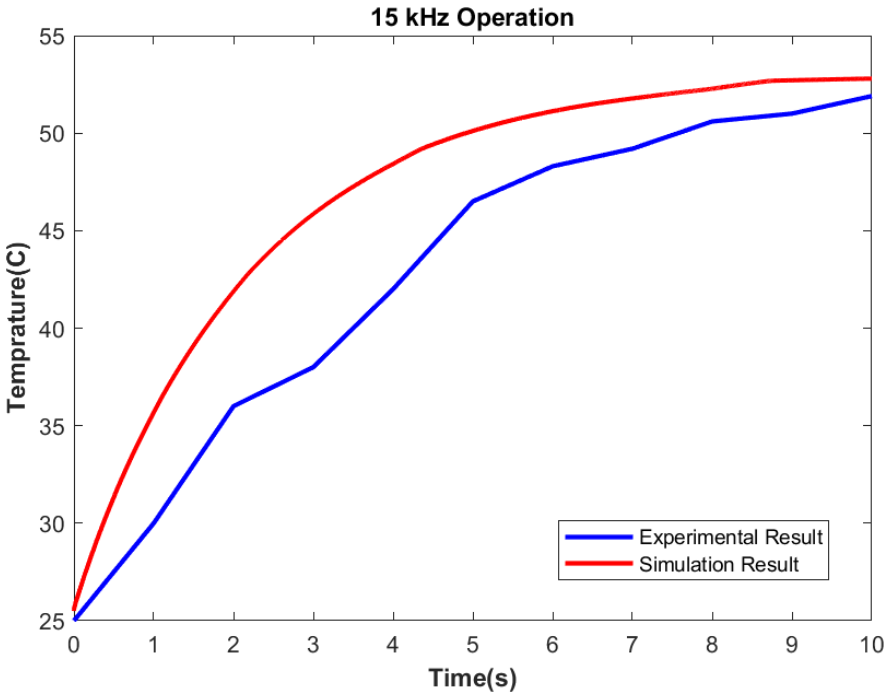

Figure 23 Switching Element Temperature Graph at 15kHz

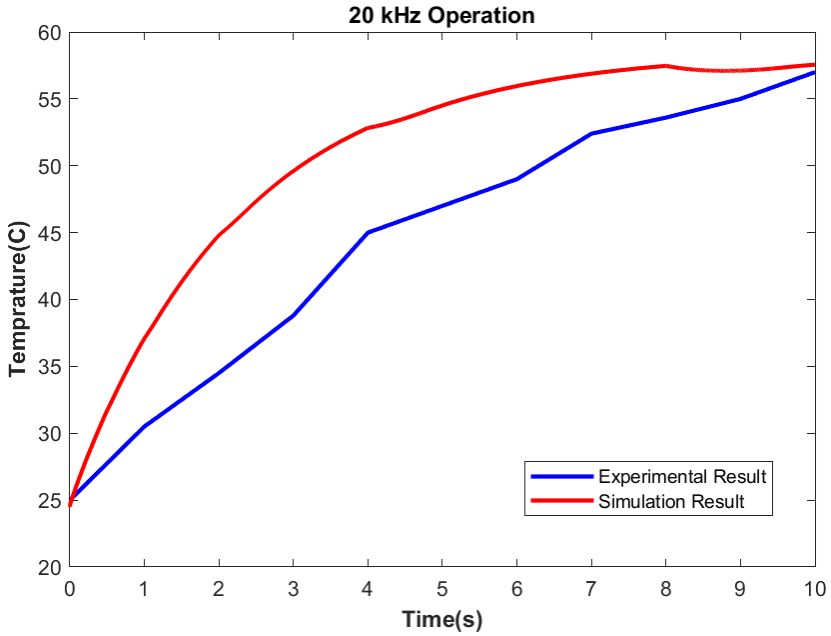

Figure 24 Switching Element Temperature Graph at 20kHz

Similarly in figure 4-2 and 4-3, the experimental results follow the same trend for temperature according to their respective simulated results. But it has been observed that the temperature after 10s is around 53°C for 15kHz and 57°C for 20kHz.

So, it has been concluded that the temperature of the switching device is temperature depended. As the frequency increase the temperature also increase because the increase in frequency can cause more switching and conduction losses, which results in higher power dissipation. Due to this power dissipation the internal and external temperature of the device increases.

4.1.2 Temperature Verification with Different Input Current

Same experimental setup is used to verify the temperature profile by applying different inputs (10V, 15V, 20V) and also by keeping the frequency of the system remains constant at 20kHz. The outcomes with respect to these inputs can be seen in figure 4-4, 4-5 and 4-6.

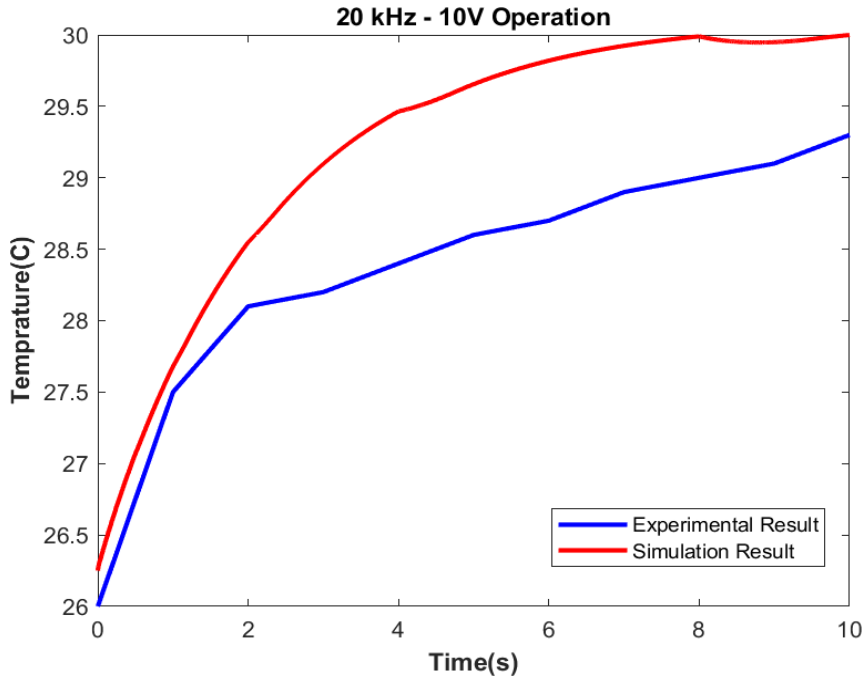

Figure 25 Switching Element Temperature Graph at 10V Input

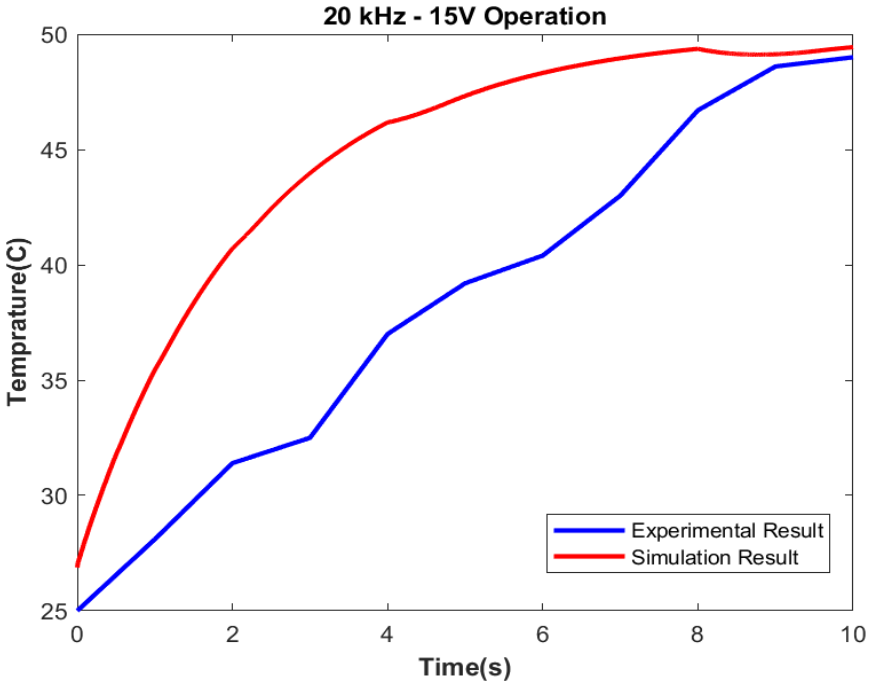

Figure 26 Switching Element Temperature Graph at 15V Input

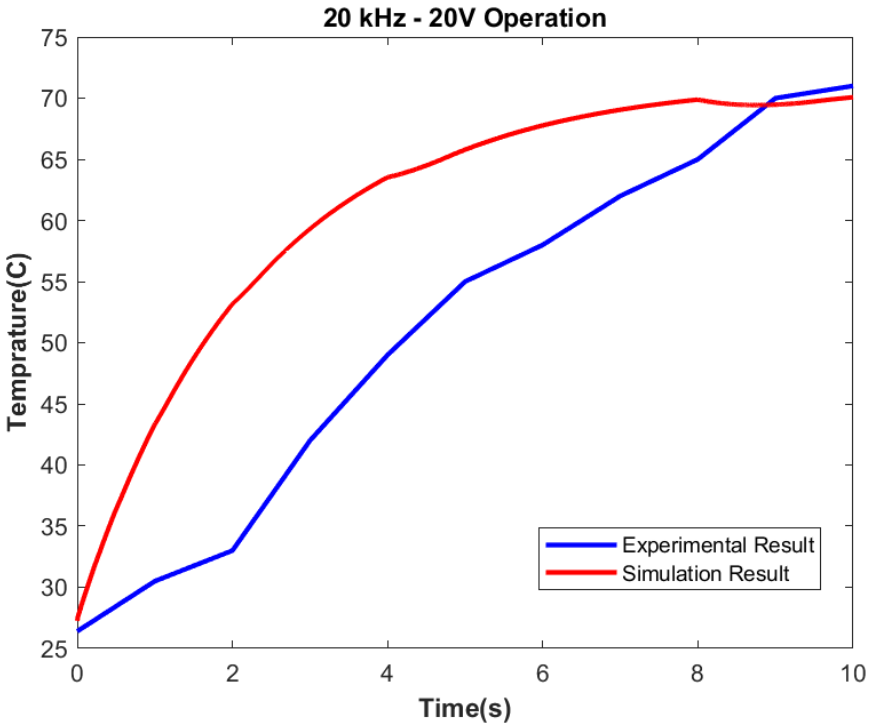

Figure 27 Switching Element Temperature Graph at 20V Input

From figure 4-4 we can analyze that the experimental and the simulated values for the temperature are almost same with the error percentage about 4% due to experimental error. The ambient temperature of both results is same around 26°C. The difference in temperature values for simulated and the experiment is around 1.5°C which is acceptable in experimental work, so it has been observed that our experimental work is verified.

Similarly goes for figure 4-5 and 4-6 in which we can see that experimental graphs follow the same trend with respect to simulated graphs. The ambient temperature for these graphs is also same but the temperature after 10s is around 49°C for 15V and around 70°C at 20V.

So, it is concluded that temperature of the switching device also depends on the input of the system. The increase in the input voltage or current can increase the temperature of the switching device as well.

4.2 Current Ripple Verification for Conventional Boost Converter

To make the converter output and the power quality at the load side better, the current of the converter has to be free from the ripples. Ripples instigate due to malfunction of MPPT or the due to harsh weathering conditions which makes PV to generate the PV output with ripples. Ripples just not only affect the power quality of the converter but, it also creates high power dissipation inside the device. due to this internal power losses other components of the converter gets heat up which causes the lifetime of the converter to be decrease.

In this section experimental results are being analyzed with respect to simulated results for input current ripples on the bases of different switching frequencies. The behavior and the effect of the different switching frequencies can be seen from figure 4-7, 4-8, 4-9 and 4-10.

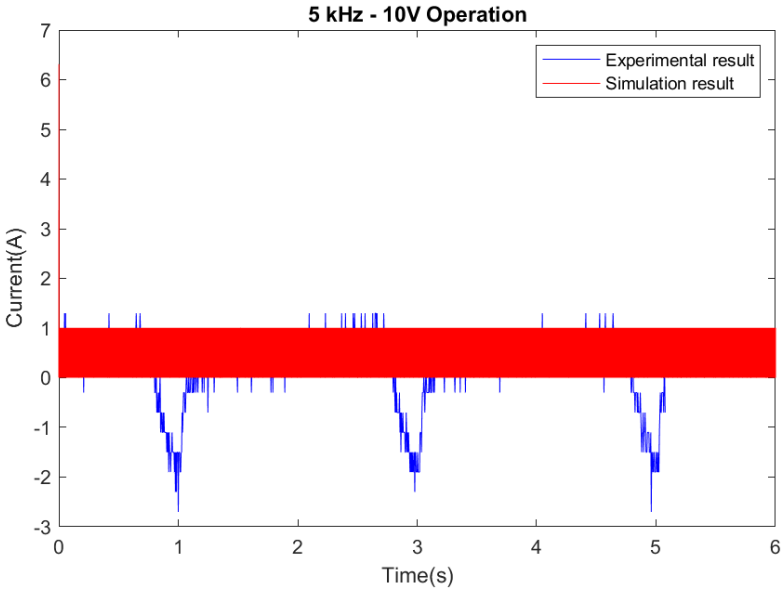

Figure 28 Current Ripples for 5kHz

Figure above compares the results of current ripples on the bases of simulations and experiment at 5 kHz. As can be observed, the ripples in the simulation are around 1A while the ripples in the experiment are about 1.3A. From an experimental standpoint, this error is acceptable because experimental data include many other characteristics and losses that were not taken into account during simulations. Our experimental findings are therefore validated with respect to simulations.

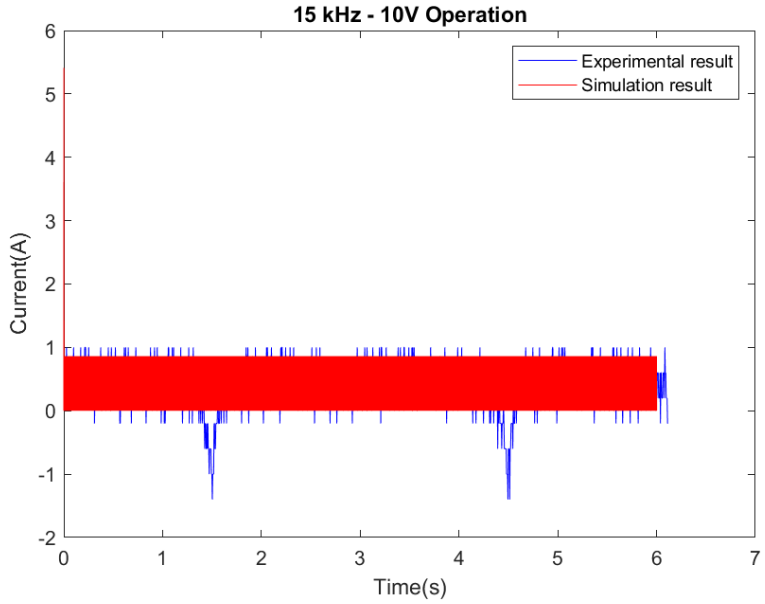

Figure 29 Current Ripples for 15kHz

It has been seen in the above figure that the current ripples have decrease as the frequency has been raised to 15 kHz. The ripples are currently around 0.9A in the simulation and around 1.2A in the experiment. Similar to what we see at 5 kHz, the amount of error in the outcome is the same.

As we increased the frequency to 20 kHz, the ripple size also shrank (see figure 4-9 below). The ripples are now only 0.25A for simulation and 0.4A for experimentation. The error margin is unchanged from earlier frequencies. Therefore, it has been determined that increasing the frequency reduced the ripples and is either one of the approaches to lower the converter's ripple to ensure smooth operation.

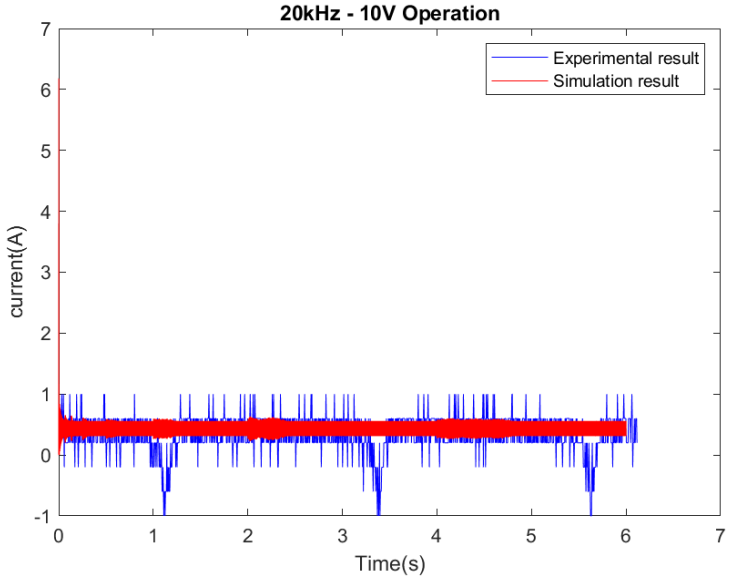

Figure 30 Current Ripples for 20kHz

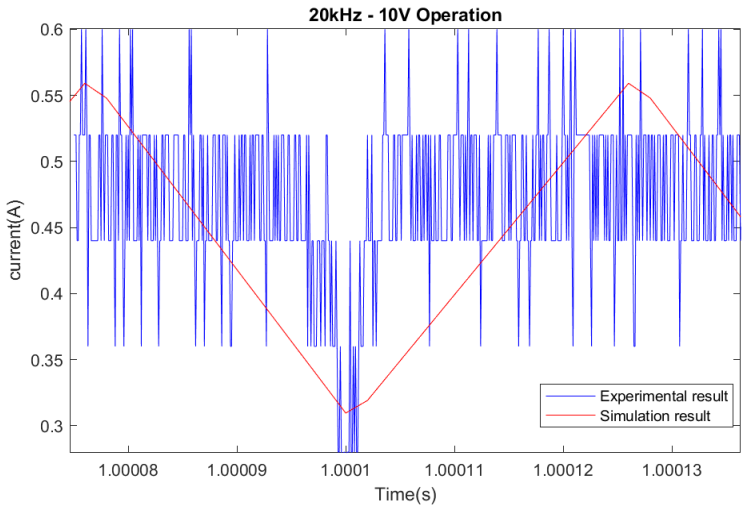

Figure 31 Zommed View of Current Ripples for 20kHz

4.3 PV-Based DC-DC Converter Simulation in MATLAB Simulink to Increase the Reliability by Variable Switching Frequency.

We use the data that was previously mentioned in the methodology section under the topic of PV modeling to simulate this model. The tilt angle must be precise according to the location if you want to get the most power out of the PV. The PV was modeled in Excel to determine the tilt angle, and 33°C was determined to be the ideal tilt angle for our campus. As stated before, this model was developed in consideration of the irradiance data gathered from the solar farm situated on our campus. Since, June 23rd was the longest day of the year, farms produced more electricity on that day, which is why the data used in this study comes from that day. The data for the is the best fit to assess the dependability of our system with a high amount of solar power because our major concern is to increase the converter's reliability.

In this research amendment has been made in the irradiance data in the form of drop of irradiance level from 890W/m^2 to 190 W/m^2 till 1.4s to 1.5s. which can be seen in figure 4-11. The purpose of this modification in the data is that in this research the model is built to perform smooth in harsh weathering condition and to maintain the temperature of the switching device constant by varying the switching frequency, so that the reliability increases and electrothermal stress should be catered.

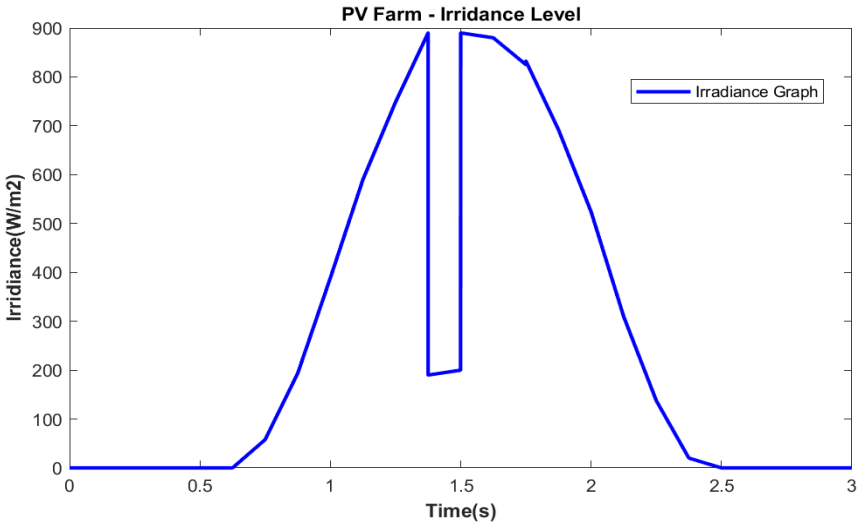

Figure 32 PV - Irradiance

4.3.1 PV Output Voltage / Converter Input Voltage

Acccording to the irridaiance the output generated by the PV can be seen in the figure 4-12, 4-13, 4-14 and 4-15. The output is generated with respect to three different fundamental switching frequencies 1kHz, 5kHz and 10kHz.

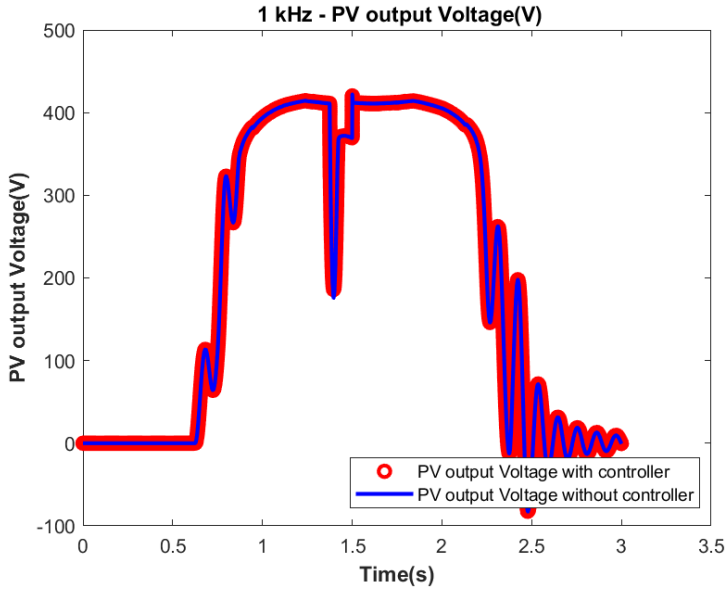

Figure 33 PV Output at 1kHz

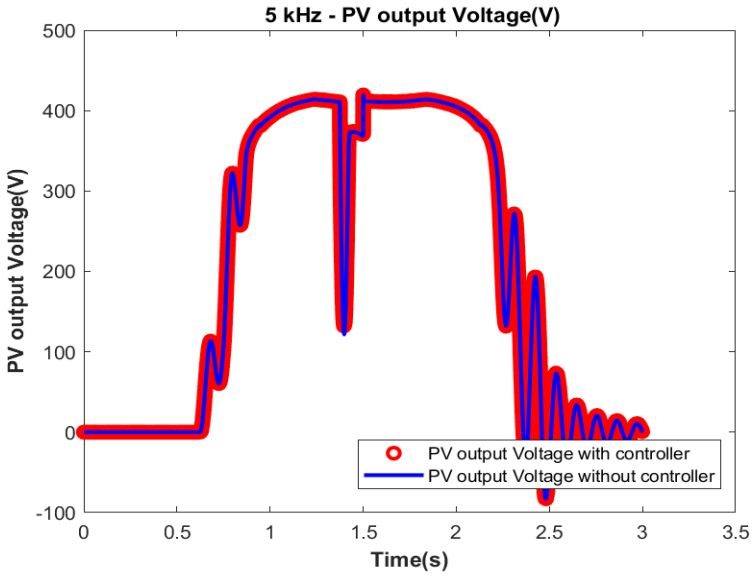

Figure 34 PV Output at 5kHz

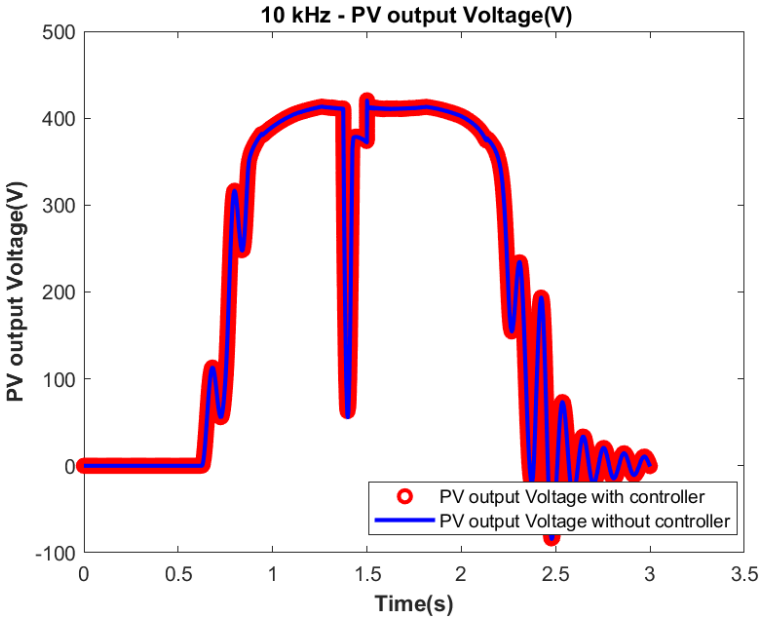

Figure 35 PV Output at 10kHz

It can be observed that the PV output is nearly same at different frequencies. The outputs have ripples and it seems unstable just because it is unfiltered output which is directly taken from PV module. The only difference in the outputs which can be analyze is the response on the drop irradiance. It can be seen that the drop at 1kHz is around 180V, at 5kHz it is around 130V and in 10kHz it is less than 100V which is quite accurate with respect to irradiance.

The output of the PV is basically the input of the converter but as we can observe the ripples in the voltage waveform. Due to these ripples, it cannot be directly attached to the input of the converter. So first it has to be pass from the low voltage capacitor which filtered out the ripples from the voltage and make the smooth waveform for the converter's operation.

4.3.2 Voltage Output at the Load End

The voltage output at the load end can be observed from the graphs below on the bases of input voltage. The input voltage of the converter is around 420V and output

of the boost converter is around 870V which validates that our boost converter with respect to the duty cycle also which is mentioned in the MPPT table 3-2. These outputs are filtered output as compare to input ones, because these voltage waveforms have passes through low voltage capacitor at the input of the converter and high voltage capacitor at the load end. These capacitor makes the out quite smooth and ripple free.

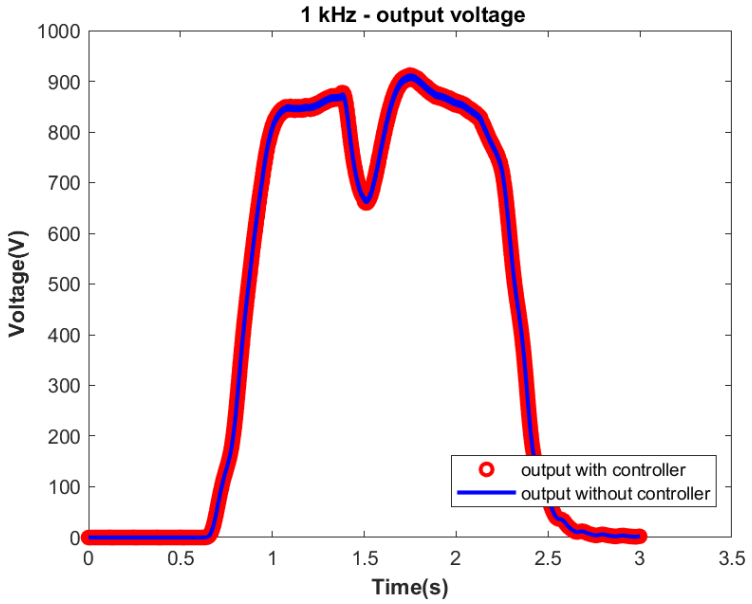

Figure 36 Voltage Output at 1kHz

The figure 4-16 above show the voltage output at 1kHz in which it has been observe that it is giving the correct output and following the irradiance trend but still we can see that the output has some ripples. The output at 1kHz is not smooth as compare to the output we achieved at 5kHz. In figure 4-17 it can also be seen that voltage has the overshoot at 1.6s to 1.7s and it takes time to stabilize itself. It means in that particular time period it didn't follow the irradiance profile.

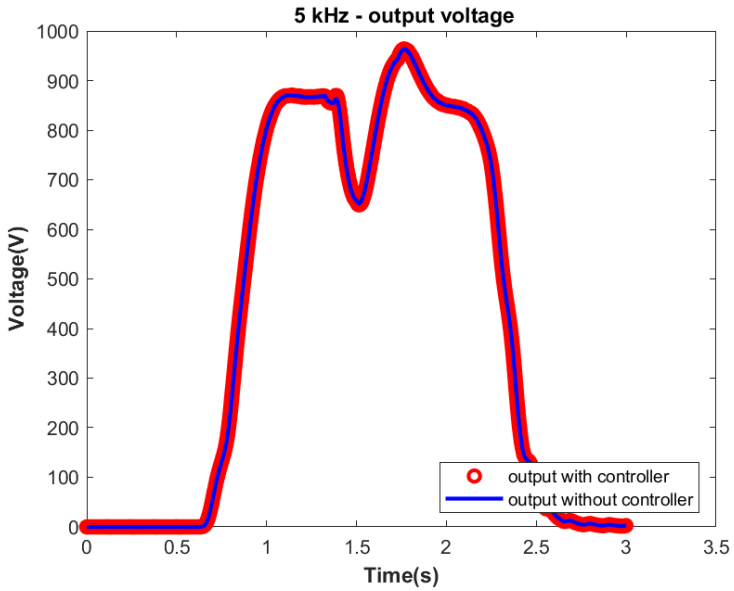

Figure 37 Voltage Output at 5kHz

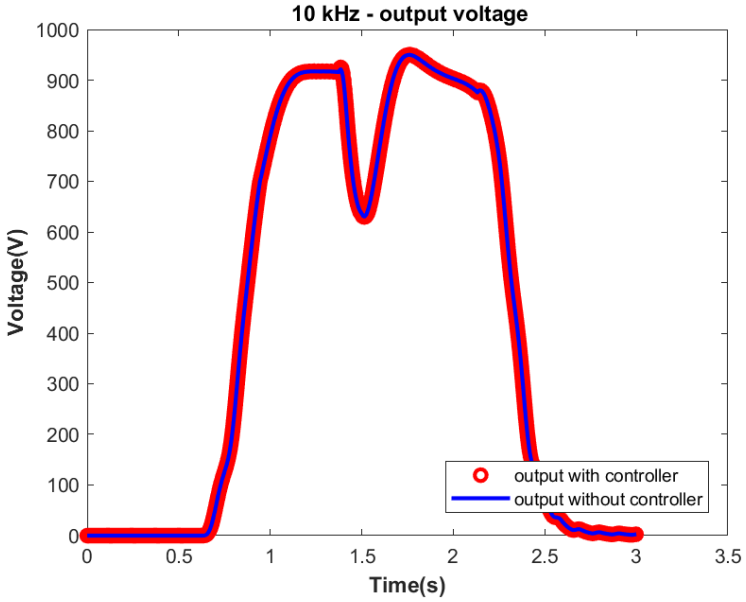

Figure 38 Voltage Output at 10kHz

As compare to 1kHz and 5kHz the voltage output at 10kHz is more smooth and ripple free. İt is following the irradiance trend accuratley without any overshoot. it concluded that increasing in the frequency can reduce the ripple in the voltage and current wave form of the system which is also validated by the experimental results in section 4.2.

4.3.3 Input Current

İnput current in the boost converter is aslo known as the inductor current whcih can bee seen in the figures 4-19, 4-20 and 4-21. İt can be observe that it following the same path as the voltage has even in comparsion of the current output from all three frequencies 10kHz has the most smooth wave form with very less ripple. The overshoot in the current is also be seen in the output of 5kHz at same time period.

The current for all the outputs are nealry same around 19A.

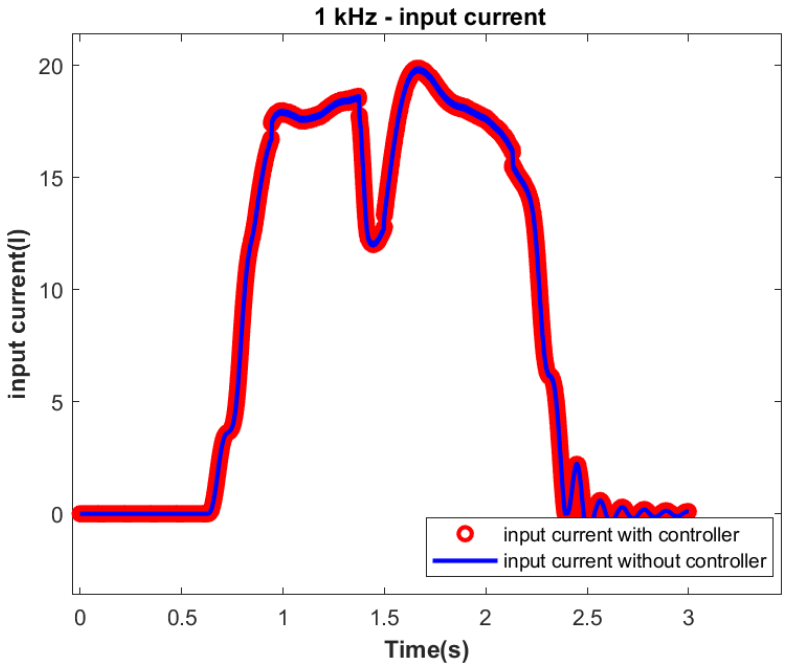

Figure 39 Input Current at 1kHz

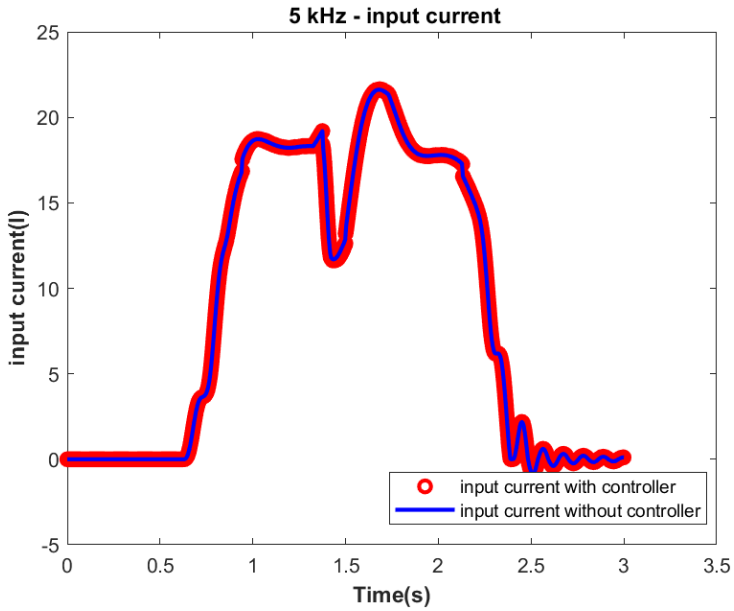

Figure 40 Input Current at 5kHz

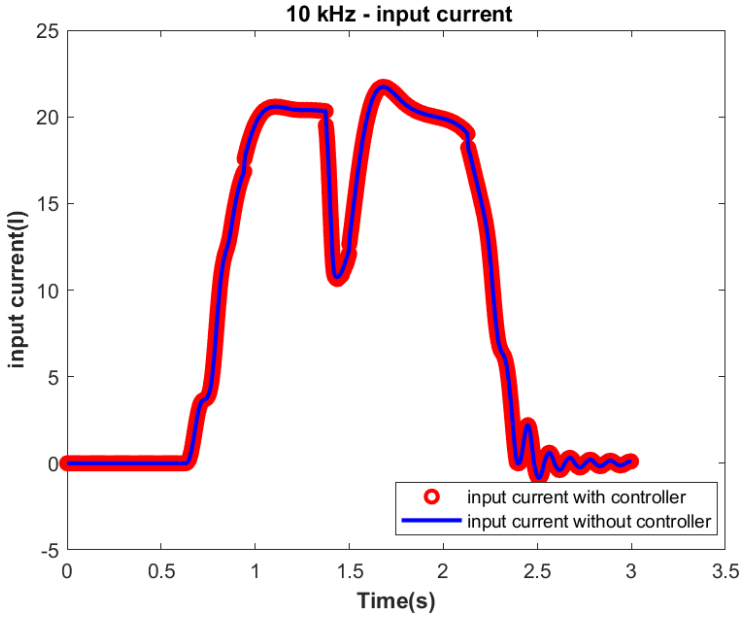

Figure 41 Input Current at 10kHz

4.3.4 Output Current

The key difference of input to output current of the converter which observe from the graphs is the amount of current decreased. The output current is comparatively half of the input current. It is the characteristic of the boost converter that at one hand it is boosting the voltage on the other hand it is doing that on the account of decreasing the current at the same rate which can be seen in figure 4-22, 4-23 and 4-24 below. The amount the current is around 9A which half as compare to input which validates the results and the design of the converter.

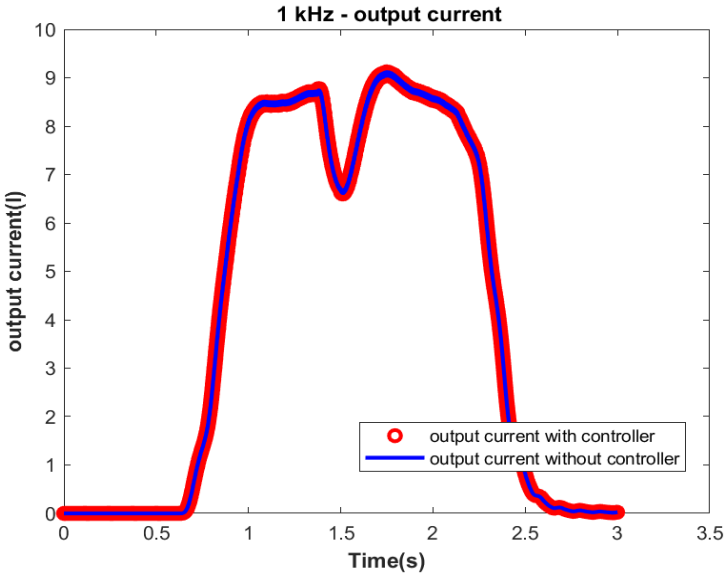

Figure 42 Current Output at 1kHz

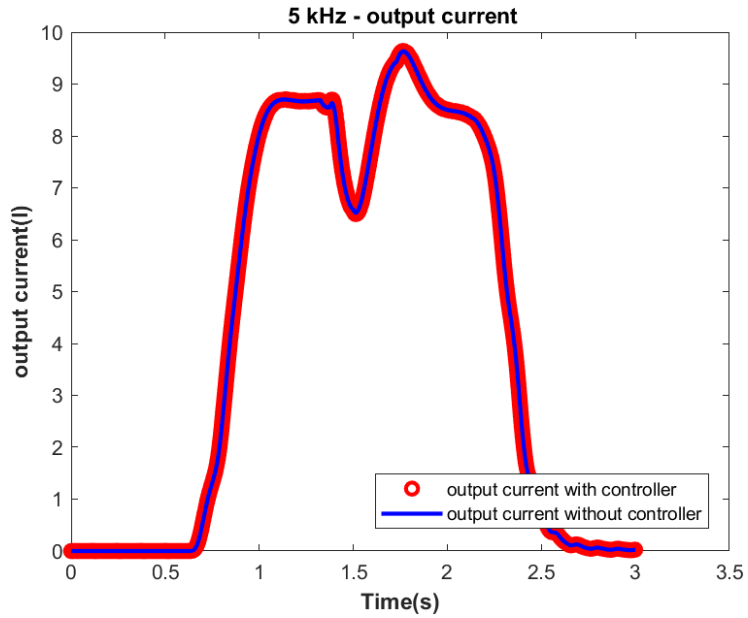

Figure 43 Current Output at 5kHz

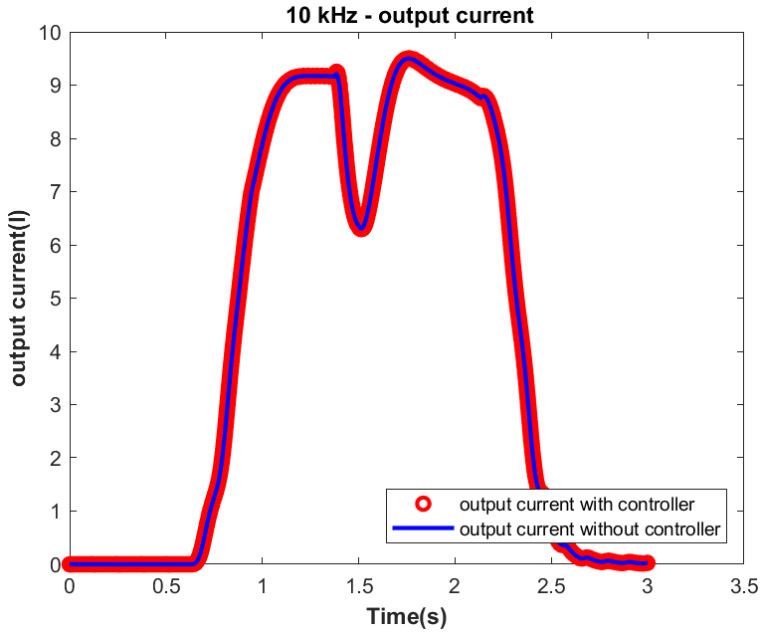

Figure 44 Current Output at 10kHz

4.3.5 Conduction Loss

The below figures 4-25, 4-26, and 4-27 show the conduction loss occurring within the device. This loss occurs when the device starts to conduct current and the device have a particular voltage drop within the device.

By comparing the results at three different frequencies it has been analyzed that the conduction loss is frequency-dependent as the frequency increase the conduction losses within the device increase. At 1kHz the loss is about 11W and respectively at 5kHz and 10kHz it is about 13W and 15W. Although it can also be seen that in lower frequency the conduction loses is drastically change its pattern while in high frequency the amount of the loss is high but it is overall have smooth transition among them.

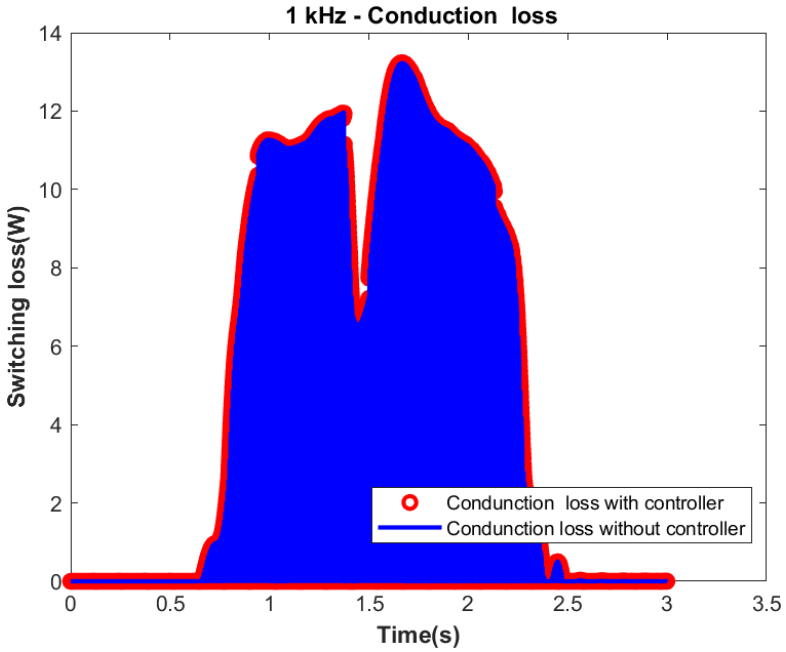

Figure 45 Conduction Loss at 1kHz

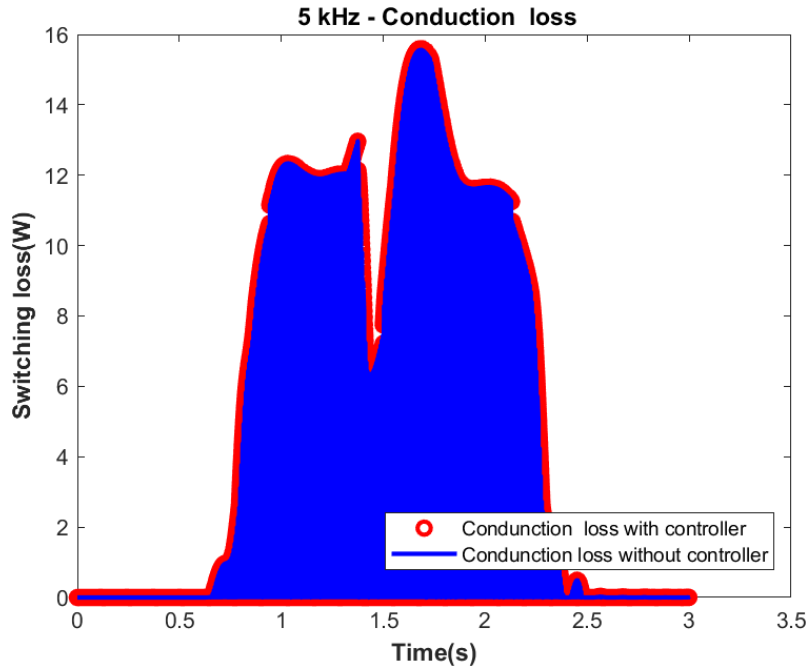

Figure 46 Conduction Loss at 5kHz

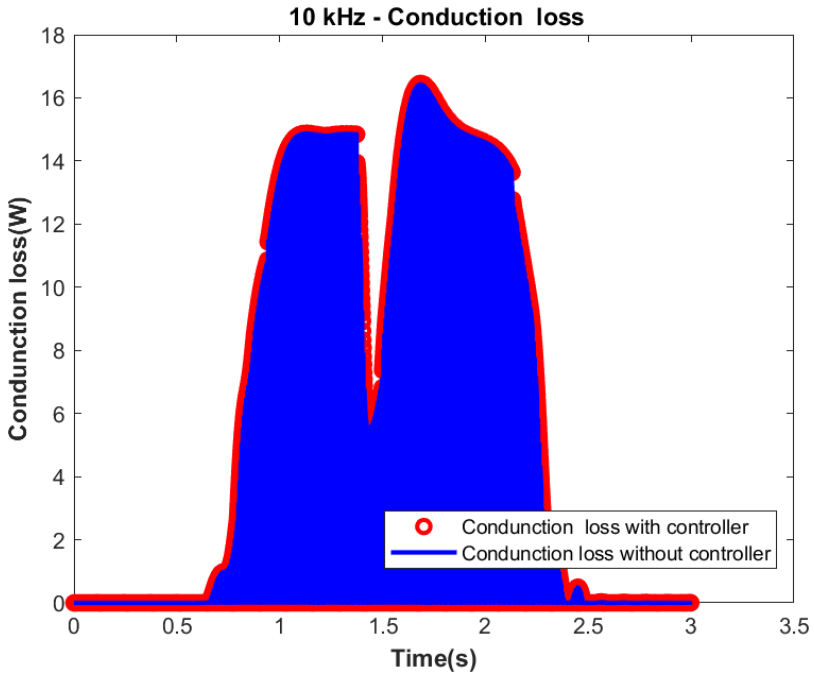

Figure 47 Conduction Loss at 10kHz

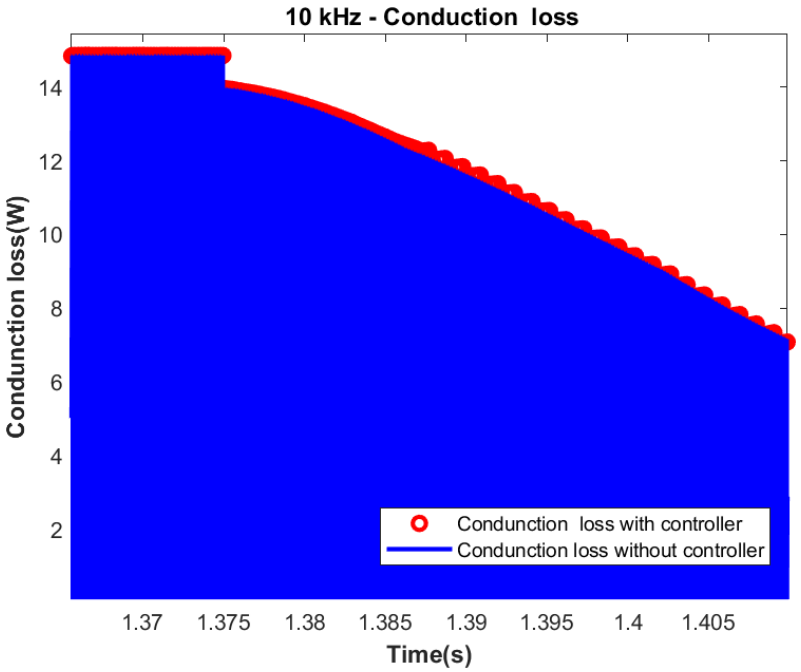

Figure 48 zoomed View for Conduction loss at 10kHz

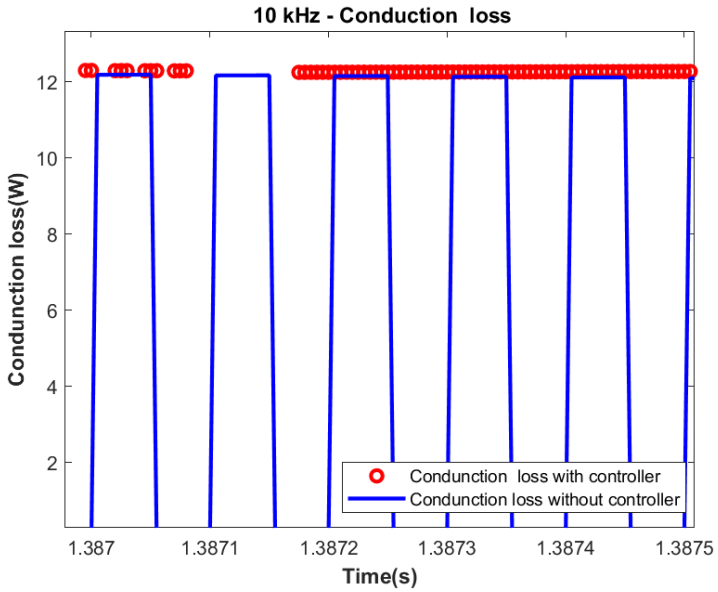

Figure 49 Zoomed view for Conduction loss at 10kHz at Sharp Change

4.3.6 Switching Loss

This section contains the results of the switching loss occur in switching element of the device while making transition from off state to on state or vice versa. The results can be observing from figures below 4-28, 4-29 and 4-30.

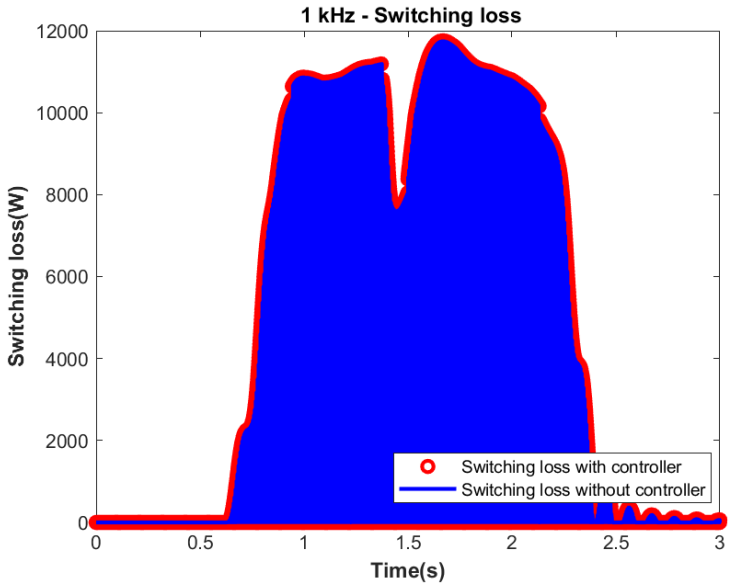

Figure 50 Switching Loss at 1kHz

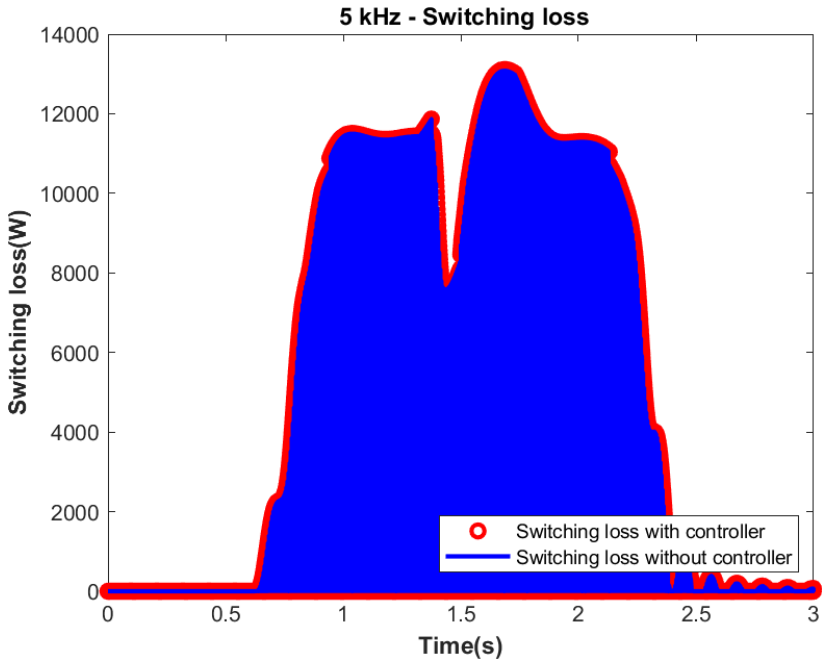

Figure 51 Switching Loss at 5kHz

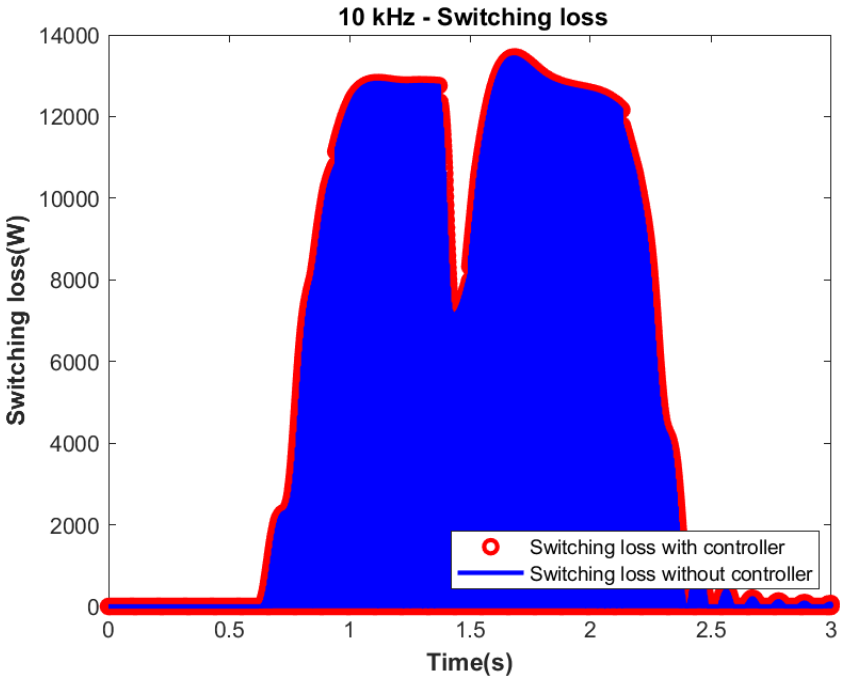

Figure 52 Switching Loss at 10kHz

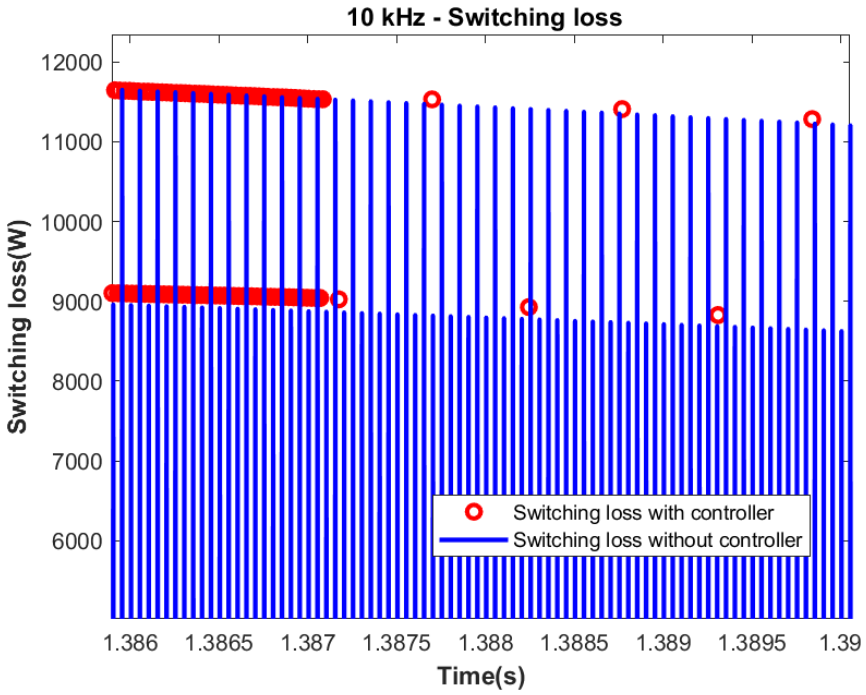

Figure 53 Zoomed View for switching loss at 10kHz

The switching loss at 1kHz can be seen around 11kW, which is not the constant amount of power loss basically it is in the form of the spike for very short period of time when the switch is changing its state, which is in milli or micro seconds. Once the transitions end then it continuous as a conduction loss till another transition occur which further explain before in section 4.3.5.

Similarly, at 5kHz and 10kHz the switching losses spikes are around 12kW and 13kW is just because the increase in frequency can increase the rate of switching due to which results in the increase of switching loss.

4.3.7 Total Power Loss

Total power loss is refereeing to the sum of all the power dissipation occur within the device at different fundamental frequencies. It can be analyzed from the 4-31 that the total power loss at 1kHz is around 22W, but it can also be observe that with the controller we have more oscillations at the time when irradiance is going down.

These oscillation occurs because at that particular time period from 1.4s to 1.6s the temperature controller become operational to make the temperature stable to avoid the electro thermal stress by varying the switching frequency with respect to its pre-defined fundamental frequency, due to which the spikes can be seen representing the switching loss.

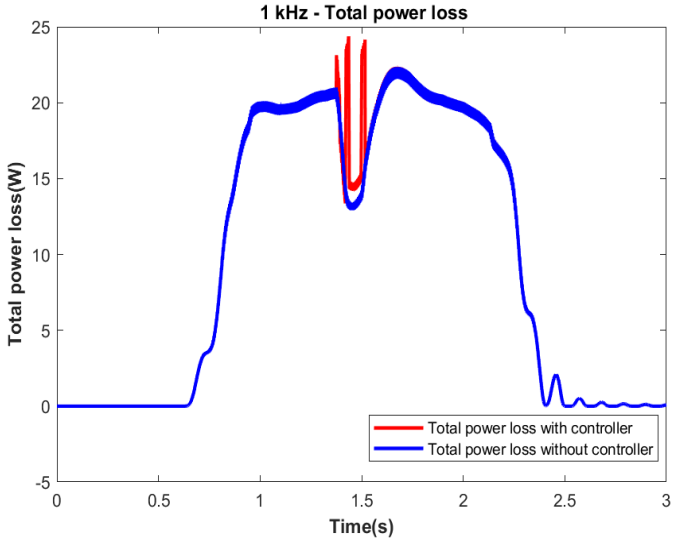

Figure 54 Total Power Loss at 1kHz

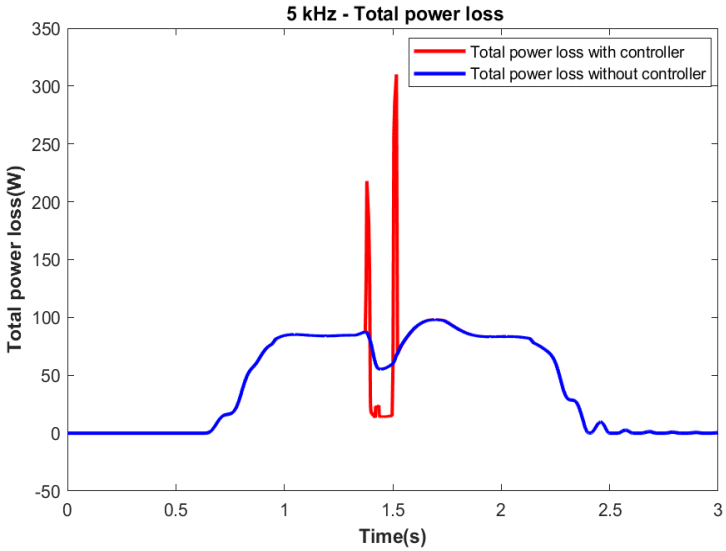

Figure 55 Total Power Loss at 5kHz

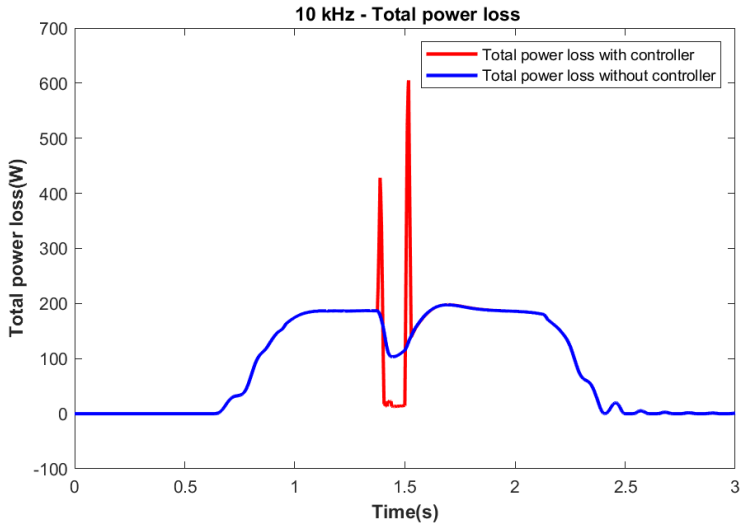

Figure 56 Total Power Loss at 10kHz

Similarly, for 5kHz and 10kHz, the total power loss is higher than 1kHz which is around 100W and 200W respectively because as we defined earlier that due to high frequency we have more conduction and switching loss which results in an increase in total power loss. It can also be observed from the above figure 4-32 and 4-33 that when the temperature controller becomes active at the time of partial shading high switching loss is observed in the form of spikes because the temperature controller consists of a variable frequency switching algorithm.

4.3.8 Power Output of the System at Load End

After the power losses and power dissipation, the power output received at the load end can be seen in figures 4-34, 4-35, and 4-36. From the graphs, it has been observed that output power follows the same trend as we got for output voltage and current, just because it is the product of these two quantities. The power outputs for all the frequency are nearly same which is 8kW. As compare to all three frequencies the output at 10kHz is much smoother and without having any overshoot.

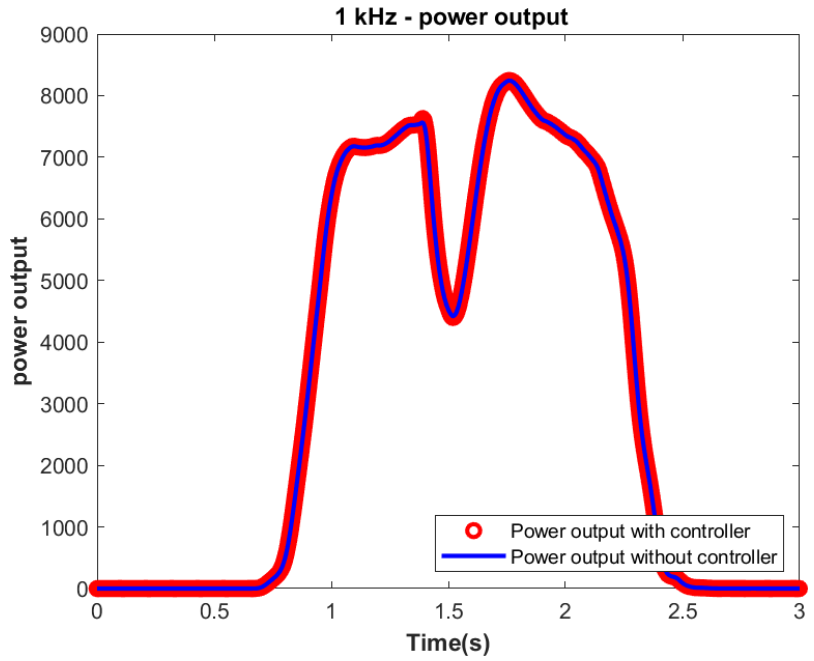

Figure 57 Power Output at 1kHz

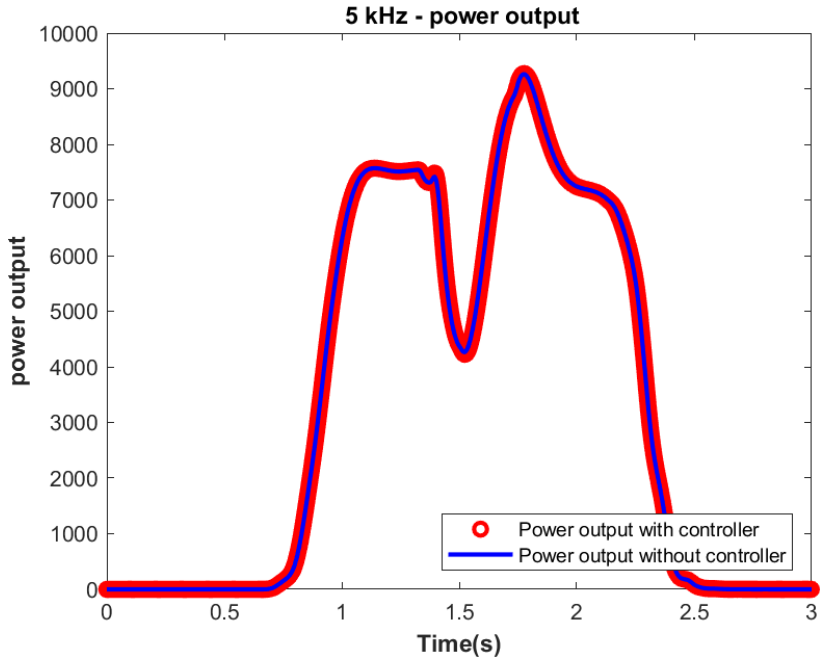

Figure 58 Power Output at 5kHz

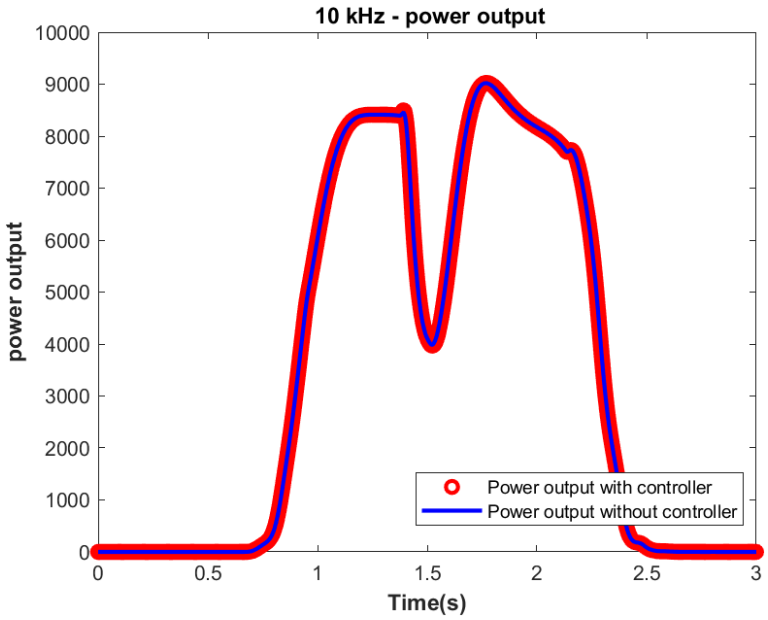

Figure 59 Power Output at 10kHz

4.3.9 Temperature Output with Respect to Frequency

The main objective of this research is to maintain the temperature of the device by using a variable switching frequency which results in increasing the reliability of the converter.

It can be analyzed from the figures 4-37 and 4-38 that when there is a huge change in temperature occur due to a change in irradiance the temperature controller varies the frequency and try to maintain the temperature. It does it by breaking the drop into smaller oscillations with higher amplitude with respect to the drop we analyze in the temperature graph without controller. Because having the small change in temperature doesn't affect the reliability of the converter much as compare huge change in temperate.

By doing so at same time period we have also observe the increase in the switching loss which is mentioned in section 4.3.7.

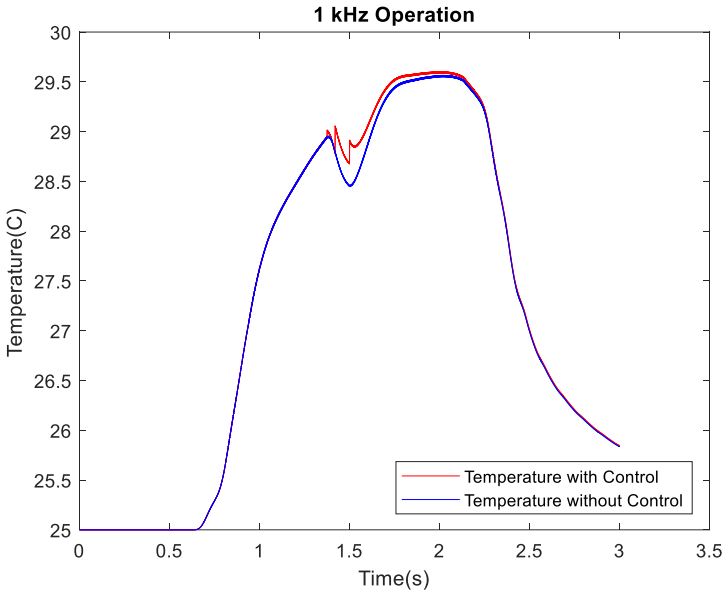

Figure 60 Temprature of Switching Element at 1kHz

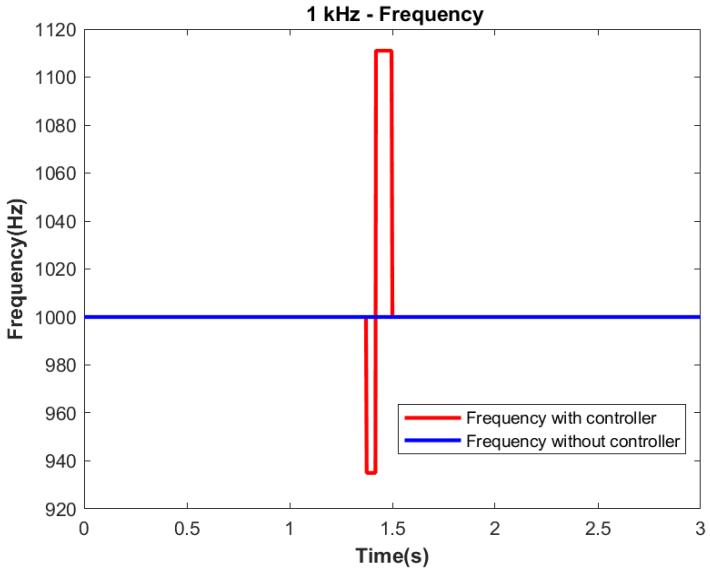

Figure 61 Frequency Response

Similarly for 5kHz the controller works in the same way to maintian the temprature of the device. The differnec is only about the amplitude of the device juntion temprature which is incerased due to incerased in ferquency.

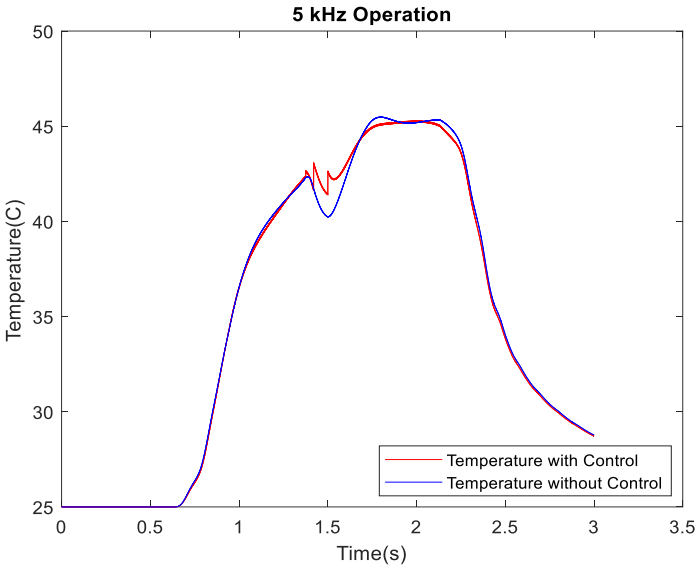

Figure 62 Temprature of Switching Element at 5kHz

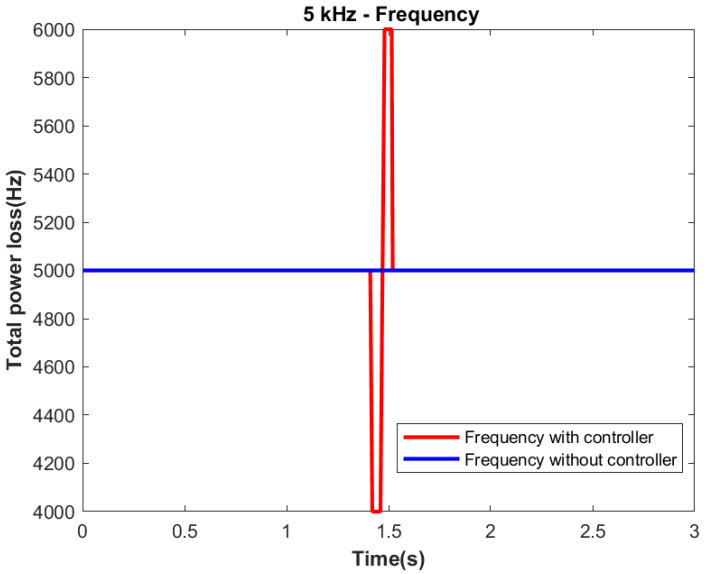

Figure 63 Frequency Response

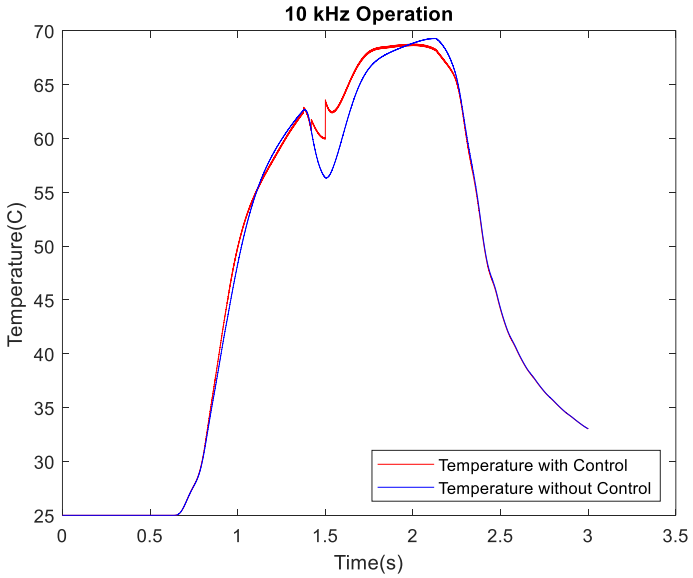

Figure 64 Temprature of Switching Element at 10kHz

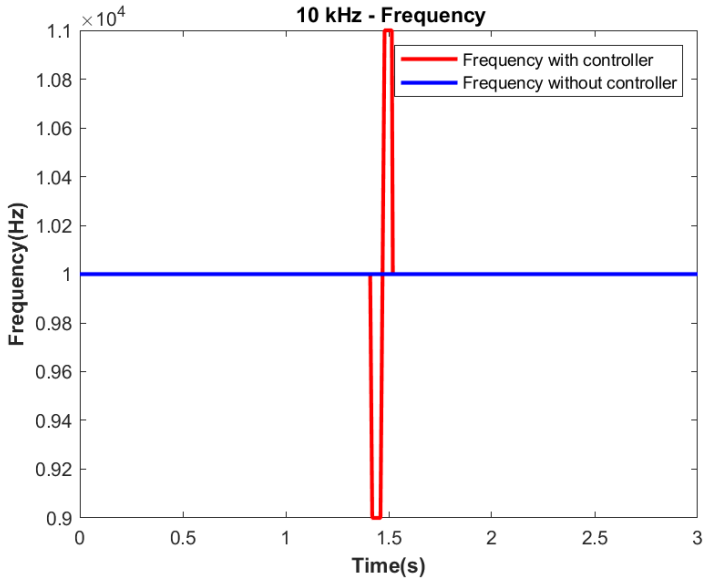

Figure 65 Frequency Response

By analyzing figure 4-41 and 4-42 it has been concluded that temprature of the switching element in 10kHz is high as compare to others which is about 68℃, but

the controller beahaves in 10kHz much more accuratley and maintain the temprature of the device with much reduced oscillations than other frequencies.

4.3.10 Representation of Reliability Using Life Time Consumption Calculations

The previous sections contain the result of power converter and its electro-thermal model to analyze the results with respect to temperature of the switching element of the device. After making the temperature profile of the switch constant with the help of the controller which varies the switching frequency, the reliability of that switching element has to be analyzed. so that it should be validate that by applying that methodology has we achieved the more life time for our device.

Weibull statists is used to observe the life time analysis for the power converters and it's done in the form of the count of the cycles in which device collapse. Therefore, to estimate the lifetime with respect to cycling temperature, we have took temperature profile of the switching element in to the account. So, in this research we adopt the Coffin Manson Arrhenius Analytical Model to observe the reliability and to estimate the life time consumption of the device. The equation for this model can be seen below.

$$N = AT^{\alpha} * e^{\frac{E}{K*t}} \tag{4.1}$$

Where N is the number of cycles to failure, T is the junction temperature of the device, K is the Boltzmann constant, t is the mean temperature, E is the activation energy, A and alpha are constant which 610 and -5.

Then the life time consumption of the device is calculated from the equation given below. It is calculated by the division of number of cycles at each temperature by the sum of the number of cycles for failure which we obtained in equation 4.1.

$$LC = \sum_{i=1}^{j} \frac{n_i}{N_i} \tag{4.2}$$

Where n is the number of cycles for each temperature. These number of cycles are extracted from temperature signal by using the MATLAB code of rain flow algorithm. The results can be analyzed in way that the least outcome of LTC has the best reliability.

These methods have been applied on three different frequencies which we use earlier to define previous results, in the similar way the reliability of the converter have been tested on those frequencies to find out at which frequency we got the high reliability for our system. The results for 1kHz without controller can be seen in the figure below. The rain flow algorithm generates the 3D graph from which we can take the values of the mean temperature, cyclic temperature and the no cycles at each temperature. After extracting and putting the values in the equations we find the LTC of the converter at 1kHz without controller is about 3.0667E-153.

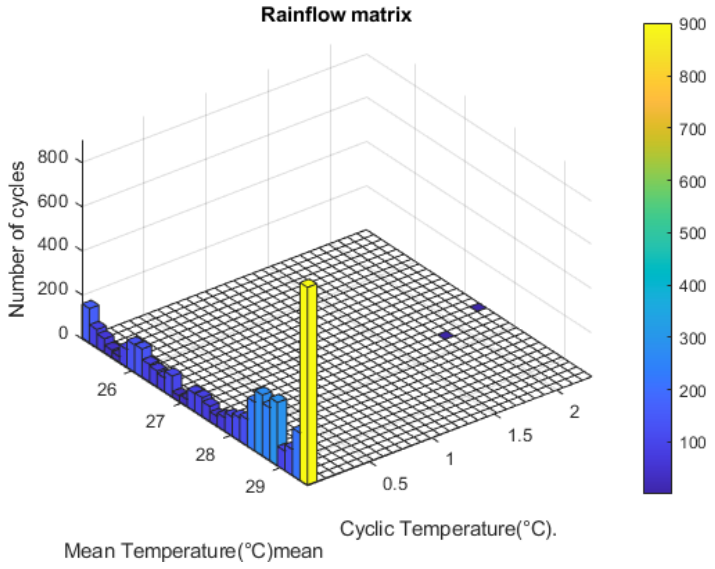

Figure 66 RainFlow Matrix for 1kHz without Controller

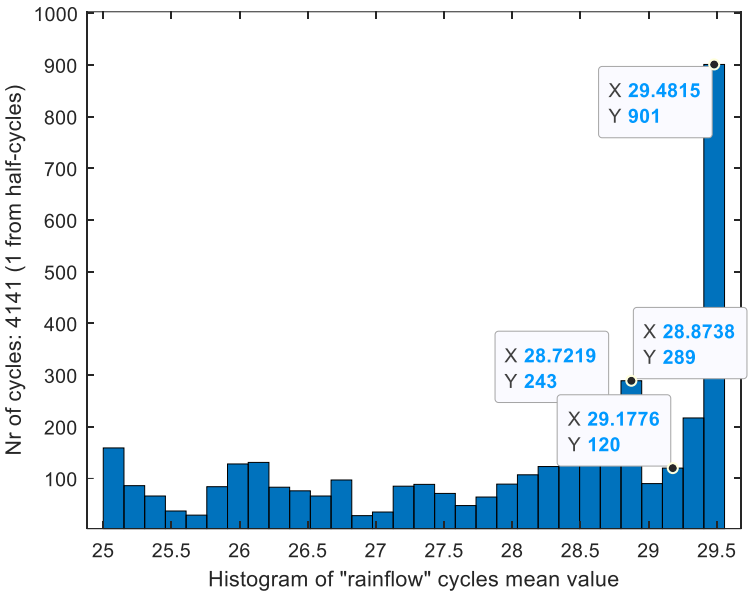

Figure 67 Histrogram for Rainflow Matriz at 1kHz without controller

For the results with respect to controller we apply the same method and the LTC at 1kHz is come out to be 1.0102E-152 and the graphs can be seen below.

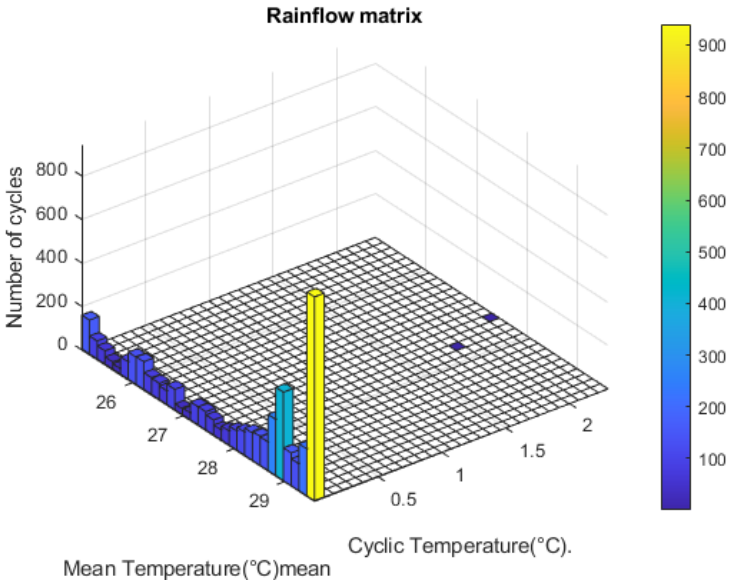

Figure 68 RainFlow Matrix for 1kHz with Controller

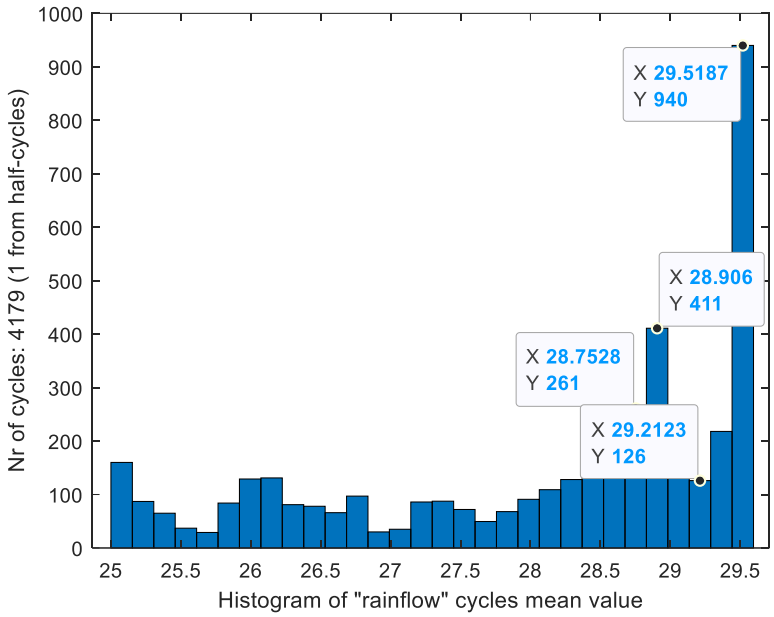

Figure 69 Histrogram for Rainflow Matriz at 1kHz with controller

From the above results it has been conclude that the converter in the 1kHz is not efficient because it has less value of LTC without controller.

The similar methodology has been applied for 5kHz and 10kHZ with and without controller. The outcome at 5kHz without controller 4.75928E-96 and without controller 2.65298E-95. The value of LTC at 5kHz with controller is quite low with controller, which state that the converter at 5kHz is working on relaible mode and the relaiblity of the converter is incresed by applying the temprature controller. The outcome at 10kHz without controller 4.75928E-96 and with controller 1.75285-95. The value of LTC at 10kHz with controller is also quite low without controller, which state that the converter at 10kHz is also working on relaible mode. The graphs for these frequencies can be seen in the appendix.

By analyzing the results, it can be concluded that the the over all relaiblity of the converter is increasing with the incresae in frequency.

CHAPTER 5

CONCLUSION

Solar systems are those that use the power of the sun to power themselves. They do this by generating electricity using photovoltaic (PV) cells or PV modules. Being one of the cleanest and most affordable energy sources among all renewable energy sources, solar electricity is a great option. PV modules produce power, which is then sent from a DC-DC converter to a DC load. It highlights the point towards DC-DC converter that if the Load need to be drive smoothly wihout an fault. The converter has to relaible. During power conversion, a variety of problems can arise, including conduction losses, switching losses, electro-thermal stress, temperature swings, and fatigue, all of which reduce the reliability of the converter. Overvoltage or short circuits in the system can be caused by electro-thermal stress and temperature fluctuations. An answer to this issue is provided by the electrothermal modeling in the system.

In this research we have modelled the PV based DC-DC converter with electrothermal model to keep an eye on the temperature and with the help of the temperature controller the temperature of the switching element made constant. When the PV faces the harsh weathering condition the controller varies the frequency to make the temperature constant at that particular time period. The electrothermal model consist of the lookup table which generates the power loss with respect to current and voltage of the switching element. Then that power loss went in to foster thermal network which generates the temperature of the device.

The modelled has been tested on the three different frequencies with or without controller and by comparing all the results, 10kHz is turned out to be the frequency on which our converter shows the high reliability and the experimental and simulation results are in the good agreement. Due to which it is concluded that running this model on high frequency can has various advantages like, less ripple, high reliability and high change in temperature to measure.

REFERENCES

[1] P. A. Østergaard, N. Duic, Y. Noorollahi, H. Mikulcic, and S. Kalogirou, "Sustainable development using renewable energy technology," *Renew. Energy*, vol. 146, pp. 2430–2437, 2020, doi: 10.1016/j.renene.2019.08.094.

[2] K. J. Frp *et al.*, "*Ulg ,Qwhjudwlrq Ri N: 6Rodu 3Dqho," pp. 257–266, 2016.

[3] G. M. S. Azevedo, M. C. Cavalcanti, K. C. Oliveira, F. A. S. Neves, and Z. D. Lins, "Comparative evaluation of maximum power point tracking methods for photovoltaic systems," *J. Sol. Energy Eng. Trans. ASME*, vol. 131, no. 3, pp. 0310061–0310068, 2009, doi: 10.1115/1.3142827.

[4] K. Ishaque, Z. Salam, and G. Lauss, "The performance of perturb and observe and incremental conductance maximum power point tracking method under dynamic weather conditions," *Appl. Energy*, vol. 119, pp. 228–236, 2014, doi: 10.1016/j.apenergy.2013.12.054.

[5] P. Electron-, "Reliability of Power Electronic Converter Systems [Member News]," *IEEE Power Electron. Mag.*, vol. 3, no. 4, pp. 62–62, 2016, doi: 10.1109/mpel.2016.2616118.

[6] S. Kurtz, "Photovoltaic Module Reliability Workshop 2011: https://www.nrel.gov/docs/fy11osti/51121.pdf," no. November, p. NREL/TP-5200-60170, 2013, [Online]. Available: https://www.nrel.gov/docs/fy11osti/51121.pdf.

[7] J. L. Afonso *et al.*, "A review on power electronics technologies for electric mobility," *Energies*, vol. 13, no. 23, 2020, doi: 10.3390/en13236343.

[8] H. Wang, K. Ma, and F. Blaabjerg, "Design for reliability of power electronic systems," *IECON Proc. (Industrial Electron. Conf.*, pp. 33–44, 2012, doi: 10.1109/IECON.2012.6388833.

[9] C. Busca *et al.*, "An overview of the reliability prediction related aspects of high power IGBTs in wind power applications," *Microelectron. Reliab.*, vol. 51, no. 9–11, pp. 1903–1907, 2011, doi: 10.1016/j.microrel.2011.06.053.

[10] Z. Hu, W. Zhang, and J. Wu, "An improved electro-thermal model to estimate the junction temperature of IGBT module," *Electron.*, vol. 8, no. 10, 2019, doi: 10.3390/electronics8101066.

[11] H. Wang and F. Blaabjerg, "Reliability of capacitors for DC-link applications in power electronic converters - An overview," *IEEE Trans. Ind. Appl.*, vol. 50, no. 5, pp. 3569–3578, 2014, doi: 10.1109/TIA.2014.2308357.

[12] K. Harada, A. Katsuki, and M. Fujiwara, "Use of ESR for Deterioration Diagnosis of Electrolytic Capacitor," *IEEE Trans. Power Electron.*, vol. 8,

no. 4, pp. 355–361, 1993, doi: 10.1109/63.261004.

[13] F. Luis and G. Moncayo, No Covariance structure analysis Title on health-related indicators in the elderly at home with a focus on subjective health. .

[14] M. Ciappa, “Selected failure mechanisms of modern power modules,” *Microelectron. Reliab.*, vol. 42, no. 4–5, pp. 653–667, 2002, doi: 10.1016/S0026-2714(02)00042-2.

[15] J. Lutz, H. Schlangenotto, U. Scheuermann, and R. De Doncker, *Packaging and Reliability of Power Devices*. 2010.

[16] H. Ye, M. Lin, and C. Basaran, “Failure modes and FEM analysis of power electronic packaging,” *Adv. Electron. Packag.*, vol. 1, pp. 417–428, 2001.

[17] D. Zhou, F. Blaabjerg, M. Lau, and M. Tonnes, “Thermal cycling overview of multi-megawatt two-level wind power converter at full grid code operation,” *IEEJ J. Ind. Appl.*, vol. 2, no. 4, pp. 173–182, 2013, doi: 10.1541/ieejjia.2.173.

[18] Y. Ren, M. Xu, J. Zhou, and F. C. Lee, “Analytical loss model of power MOSFET,” *IEEE Trans. Power Electron.*, vol. 21, no. 2, pp. 310–319, 2006, doi: 10.1109/TPEL.2005.869743.

[19] A. Blinov, D. Vinnikov, and T. Jalakas, “Loss calculation methods of half-bridge square-wave inverters,” *Elektronika ir Elektrotechnika*, no. 7. pp. 9–14, 2011, doi: 10.5755/j01.eee.113.7.604.

[20] R. Wu *et al.*, “A power loss calculation method of IGBT three-phase SPWM converter,” *Proc. - 2012 Int. Conf. Intell. Syst. Des. Eng. Appl. ISDEA 2012*, no. 1, pp. 1180–1183, 2012, doi: 10.1109/ISdea.2012.554.

[21] V. Ivakhno, V. V. Zamaruiev, and O. Ilina, “Estimation of Semiconductor Switching Losses under Hard Switching using Matlab/Simulink Subsystem,” *Electr. Control Commun. Eng.*, vol. 2, no. 1, pp. 20–26, 2013, doi: 10.2478/ecce-2013-0003.

[22] MathWorks, “Curve Fitting Toolbox Documentation: smooth.” 2016, [Online]. Available: http://www.mathworks.com/help/curvefit/smooth.html.

[23] Z. Zhou, M. S. Kanniche, S. G. Butcup, and P. Igic, “High-speed electro-thermal simulation model of inverter power modules for hybrid vehicles,” *IET Electr. Power Appl.*, vol. 5, no. 8, pp. 636–643, 2011, doi: 10.1049/iet-epa.2011.0048.

[24] I. R. Swan, A. T. Bryant, and P. A. Mawby, “Fast thermal models for power device packaging,” *Conf. Rec. - IAS Annu. Meet. (IEEE Ind. Appl. Soc.*, pp. 1–8, 2008, doi: 10.1109/08IAS.2008.359.

[25] J. J. Barnes and R. J. Lomax, “Finite-Element Methods in Semiconductor Device Simulation,” *IEEE Trans. Electron Devices*, vol. 24, no. 8, pp. 1082–

1089, 1977, doi: 10.1109/T-ED.1977.18880.

[26] J. R. Calham, M. M. Yovanovich, and T. F. Lemczyk, “Thermal Characterization of electronic pacakges using a three-Dimensional fourier series solution,” *J. Electron. Packag. Trans. ASME*, vol. 122, no. 3, pp. 223–239, 2000, doi: 10.1115/1.1287928.

[27] D. Zhou, F. Blaabjerg, M. Lau, and M. Tonnes, “Thermal analysis of multi-MW two-level wind power converter,” *IECON Proc. (Industrial Electron. Conf.*, pp. 5858–5864, 2012, doi: 10.1109/IECON.2012.6389126.

[28] P. E. Bagnoli, C. Casarosa, M. Ciampi, and E. Dallago, “Thermal Resistance Analysis By Induced Transient (TRAIT) method for power electronic devices thermal characterization - Part I: Fundamentals and theory,” *IEEE Trans. Power Electron.*, vol. 13, no. 6, pp. 1208–1219, 1998, doi: 10.1109/63.728348.

[29] C. Tian, Y. Tan, J. Wu, and J. Li, “Thermal Network Model of IGBT Module Based on the Influence of Temperature,” *ICEMPE 2021 - 3rd Int. Conf. Electr. Mater. Power Equip.*, 2021, doi: 10.1109/ICEMPE51623.2021.9509201.

[30] D. Iru, U. Wkh, L. Ri, and S. Ghqvlw, “0Rghoolqj Wkh &Dxhu 7Khupdo 1Hwzrun Iru 3Uhvv 3Dfn ,*%7V,” pp. 7–9.

[31] “IET Power Electronics - 2020 - Yuan - Improved Cauer thermal network considering thermal coupling effects of multi-chip.pdf.” .

[32] R. Menozzi, P. Cova, N. Delmonte, F. Giuliani, and G. Sozzi, “Thermal and electro-thermal modeling of components and systems: A review of the research at the University of Parma,” *Facta Univ. - Ser. Electron. Energ.*, vol. 28, no. 3, pp. 325–344, 2015, doi: 10.2298/fuee1503325m.

[33] Y. Bulut and K. Pandya, “Thermal modeling for power MOSFETs in DC/DC applications,” *Proc. 5th Int. Conf. Therm. Mech. Simul. Exp. Microelectron. Microsystems, EuroSimE 2004*, pp. 429–433, 2004, doi: 10.1109/esime.2004.1304074.

[34] A. A. Merrikh and A. J. McNamara, “Parametric evaluation of foster RC-network for predicting transient evolution of natural convection and radiation around a flat plate,” *Thermomechanical Phenom. Electron. Syst. -Proceedings Intersoc. Conf.*, pp. 1011–1018, 2014, doi: 10.1109/ITHERM.2014.6892392.

[35] K. Ma, N. He, M. Liserre, and F. Blaabjerg, “Frequency-Domain Thermal Modeling and Characterization of Power Semiconductor Devices,” *IEEE Trans. Power Electron.*, vol. 31, no. 10, pp. 7183–7193, 2016, doi: 10.1109/TPEL.2015.2509506.

[36] X. Fan, Y. Wang, and W. Li, “Modeling and Analysis of IGBT Power Module Electro-thermal Coupling Model,” *Proc. 2021 IEEE 4th Int. Electr. Energy*

Conf. CIEEC 2021, 2021, doi: 10.1109/CIEEC50170.2021.9510292.

[37] C. Batunlu and A. Albarbar, "Towards more reliable renewable power systems - Thermal performance evaluation of DC/DC boost converters switching devices," *Int. J. Power Electron. Drive Syst.*, vol. 6, no. 4, pp. 876–887, 2015, doi: 10.11591/ijpeds.v6.i4.pp876-887.

[38] "REDAR - METU NCC Renewable Energy Research." [Online]. Available: http://redar.ncc.metu.edu.tr/.

[39] J. A. D. Deceased and W. A. Beckman, *Solar engineering of thermal processes*, vol. 3, no. 3. 1982.

[40] G. Panayiotou, S. Kalogirou, and S. Tassou, "Design and simulation of a PV and a PV-Wind standalone energy system to power a household application," *Renew. Energy*, vol. 37, no. 1, pp. 355–363, 2012, doi: 10.1016/j.renene.2011.06.038.

[41] X. Yue, D. Geng, Q. Chen, Y. Zheng, G. Gao, and L. Xu, "2-D lookup table based MPPT: Another choice of improving the generating capacity of a wave power system," *Renew. Energy*, vol. 179, pp. 625–640, 2021, doi: 10.1016/j.renene.2021.07.043.

[42] V. R. Kota and M. N. Bhukya, "A simple and efficient MPPT scheme for PV module using 2-Dimensional lookup table," *2016 IEEE Power Energy Conf. Illinois, PECI 2016*, pp. 2–8, 2016, doi: 10.1109/PECI.2016.7459226.

[43] B. M. Hasaneen and A. A. E. Mohammed, "DESIGN AND SIMULATION OF DC / DC BOOST CONVERTER," pp. 335–340, 2008.

[44] P. J. Api, "PDF File Format Java Solution."

[45] A. Fathah, "Design of a Boost Converter," *Fathah, A. (2013). Des. a Boost Convert. 2. Retrieved from http//ethesis.nitrkl.ac.in/4811/1/109EE0612.pdf*, p. 2, 2013, [Online]. Available: http://ethesis.nitrkl.ac.in/4811/1/109EE0612.pdf.

[46] S. Panich, "Design and Simulation of," *J. Med. Res.*, vol. 12, no. 3, pp. 30–40, 2012.

[47] C. Batunlu and A. Albarbar, "A technique for mitigating thermal stress and extending life cycle of power electronic converters used for wind turbines," *Electron.* , vol. 4, no. 4, pp. 947–968, 2015, doi: 10.3390/electronics4040947.

[48] C. Batunlu and A. Albarbar, "Real-time system for monitoring the electro-thermal behaviour of power electronic devices used in boost converters," *Microelectron. Reliab.*, vol. 62, pp. 82–90, 2016, doi: 10.1016/j.microrel.2016.03.033.

[49] H. Chen, B. Ji, V. Pickert, and W. Cao, "Real-time temperature estimation for power MOSFETs considering thermal aging effects," *IEEE Trans. Device*

Mater. Reliab., vol. 14, no. 1, pp. 220–228, 2014, doi: 10.1109/TDMR.2013.2292547.

[50] C. Batunlu, M. Alrweq, and A. Albarbar, “Effects of power tracking algorithms on lifetime of power electronic devices used in solar systems,” *Energies*, vol. 9, no. 11, 2016, doi: 10.3390/en9110884.

APPENDICES

A. Rain Flow Analysis for 5kHz and 10kHz

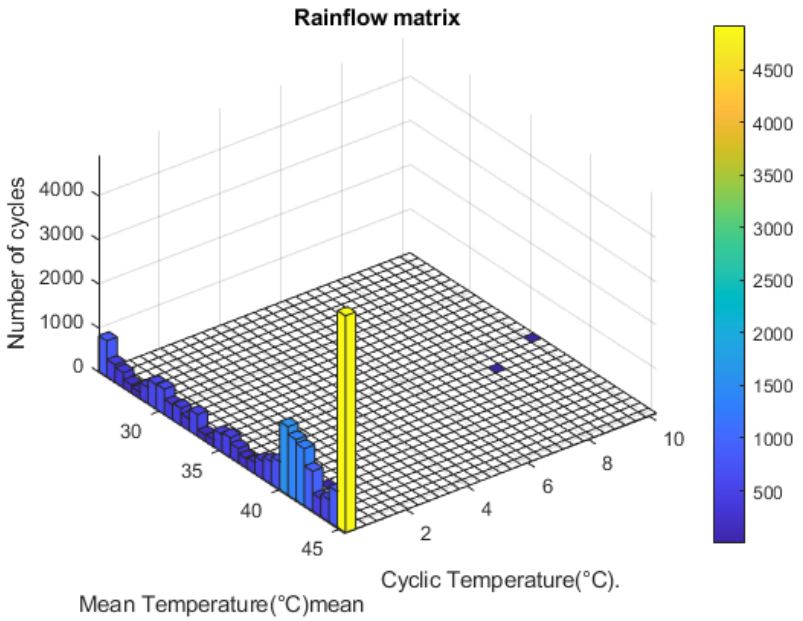

Figure A-1 5kHz Without Control

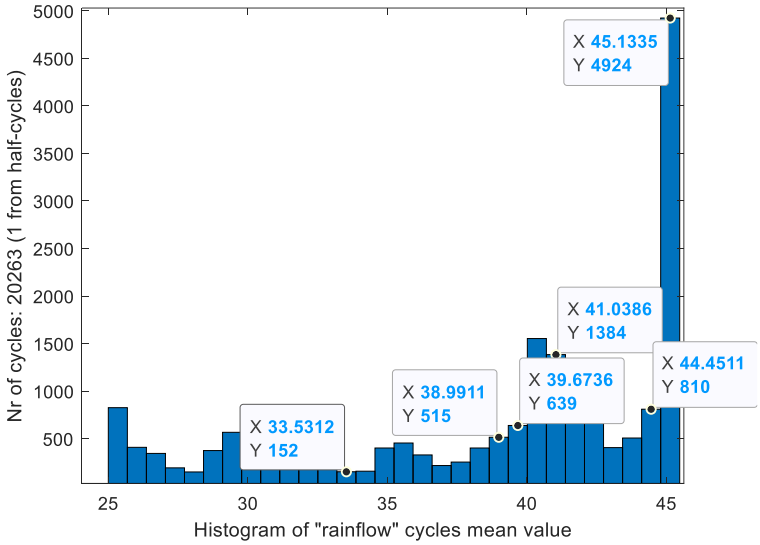

Figure A-70 5kHz Without Control

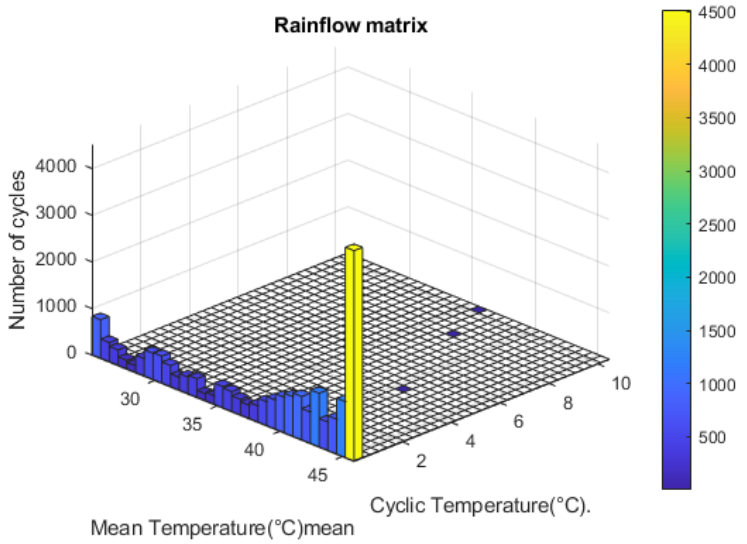

Figure A-71 5kHz With Control

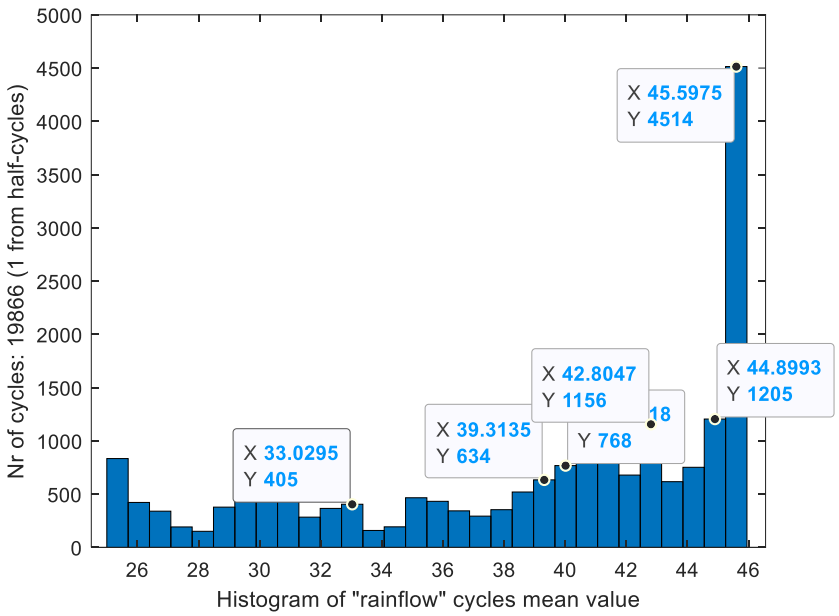

Figure A-72 5kHz With Control

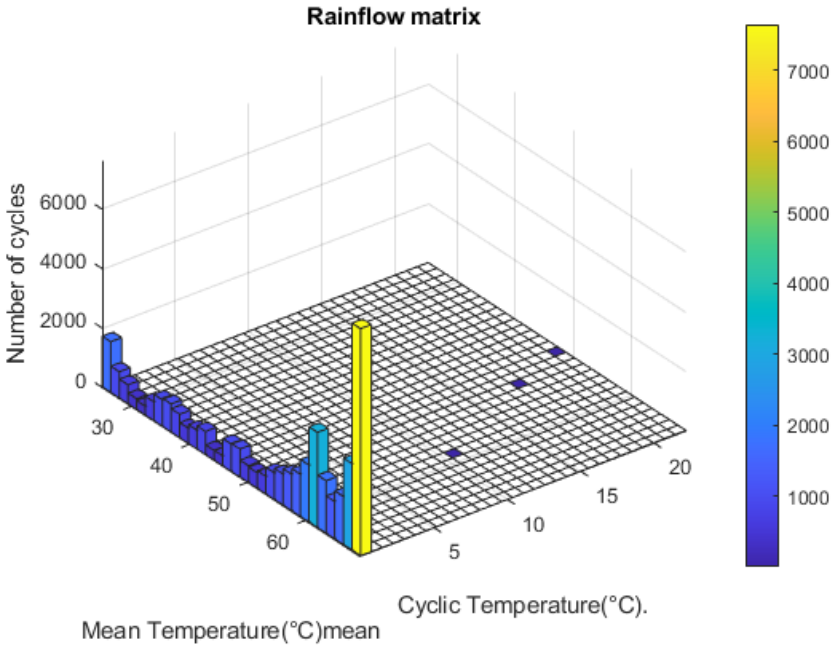

Figure A-73 10kHz Without Control

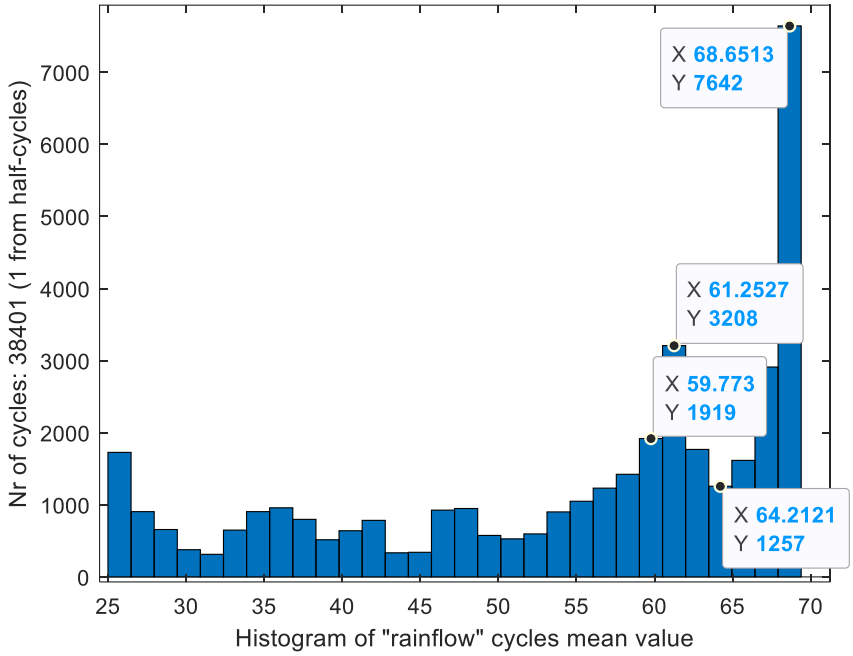

Figure A-74 10kHz Without Control

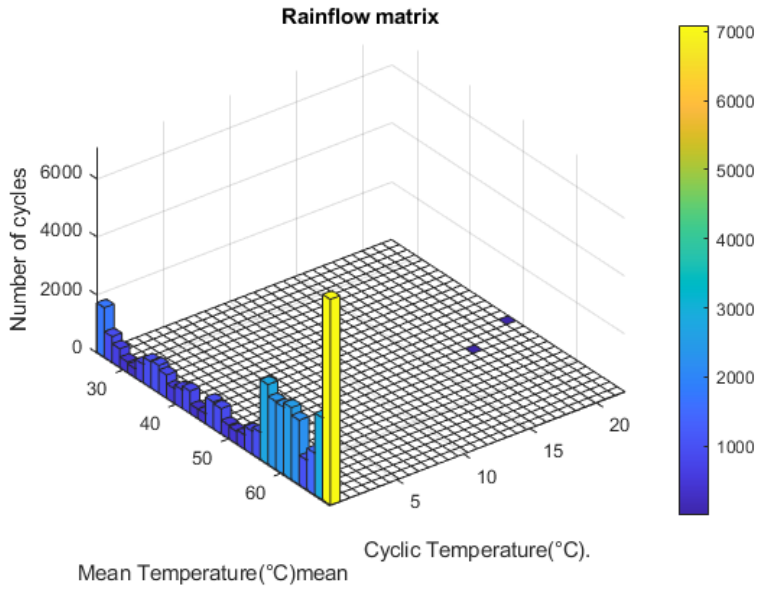

Figure A-75 10kHz With Control

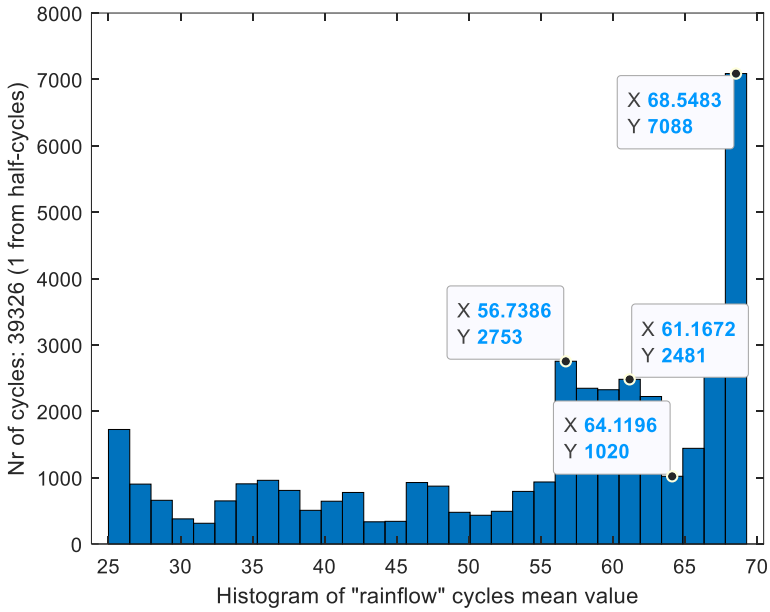

Figure A-76 10kHz With Control

B. Temprature graphs and Rain flow analysis for 15kHz and 20kHz

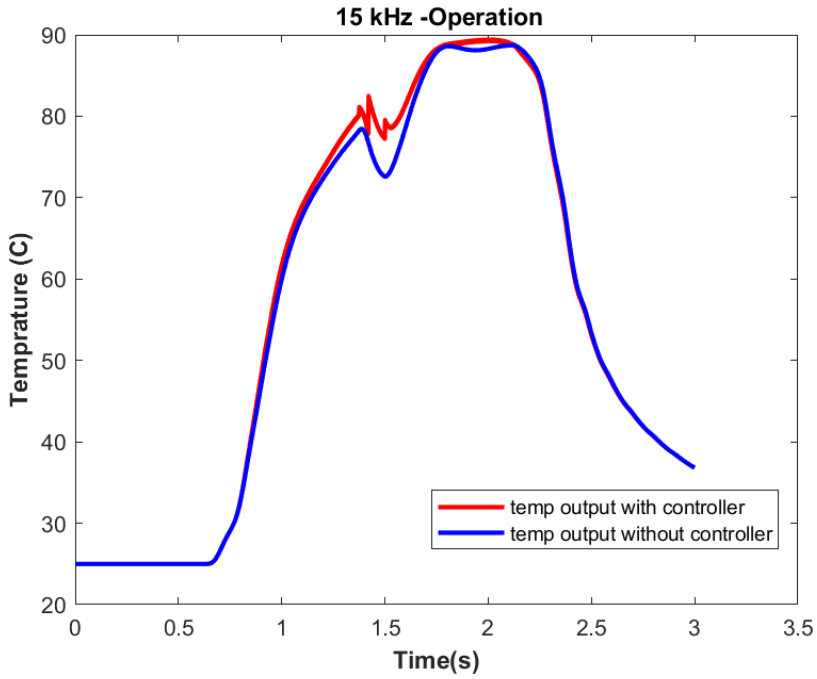

Figure B- 1 Temprature Graph for 15kHz

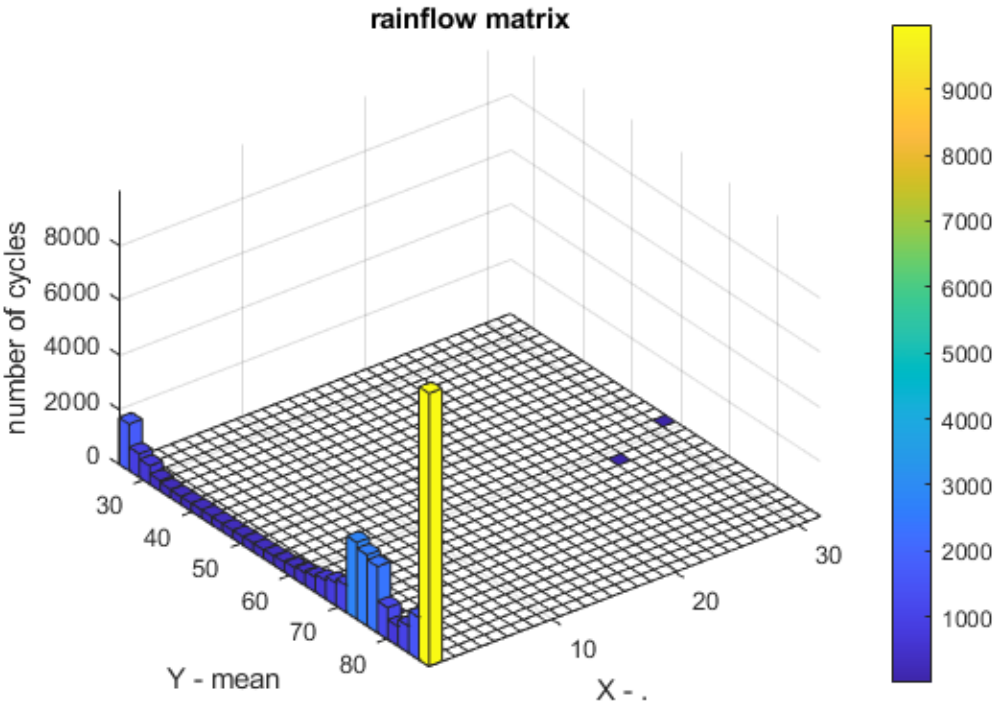

Figure B- 2 15kHz Without Control

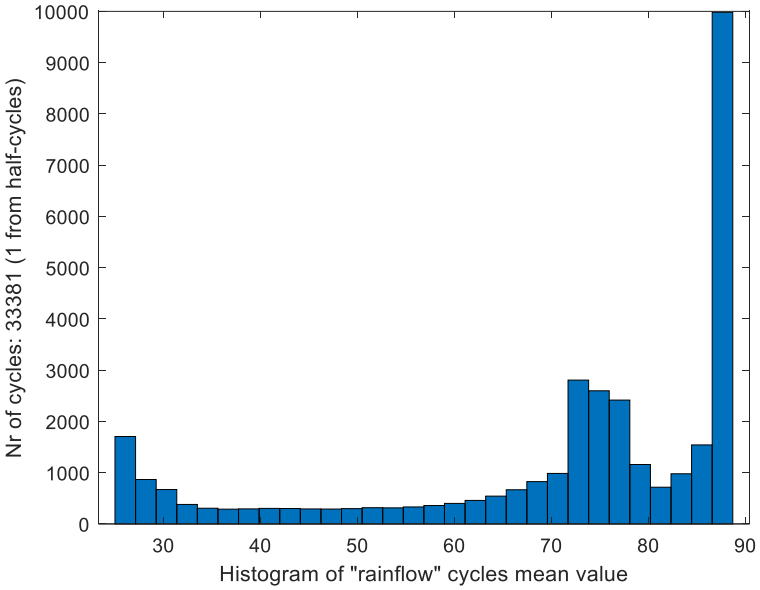

Figure B- 3 15kHz Without Control

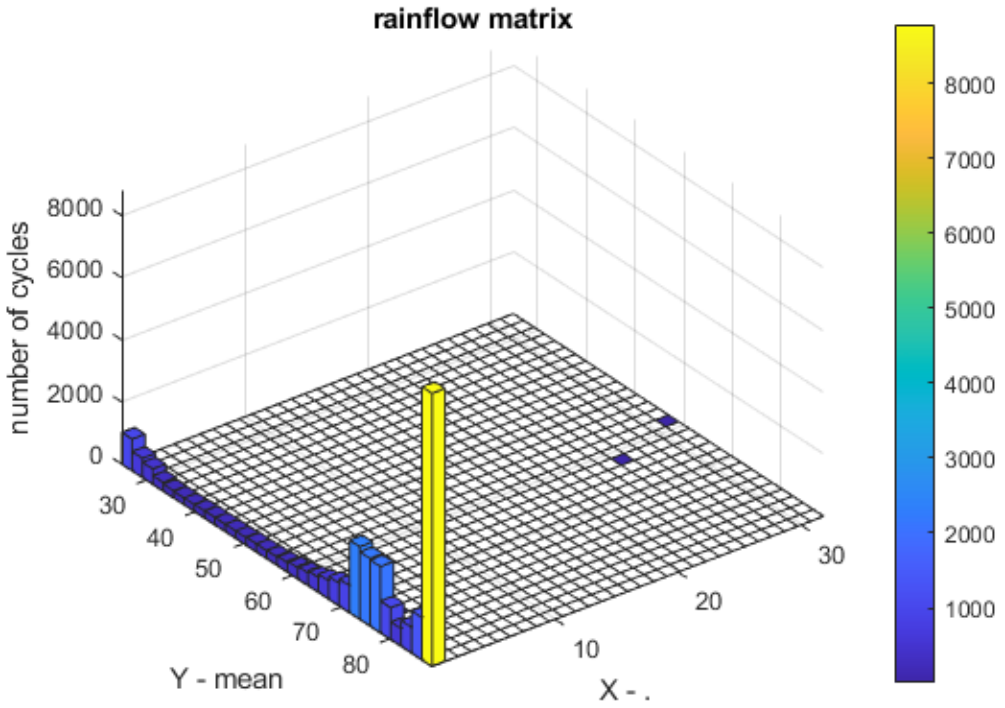

Figure B- 4 15kHz With Control

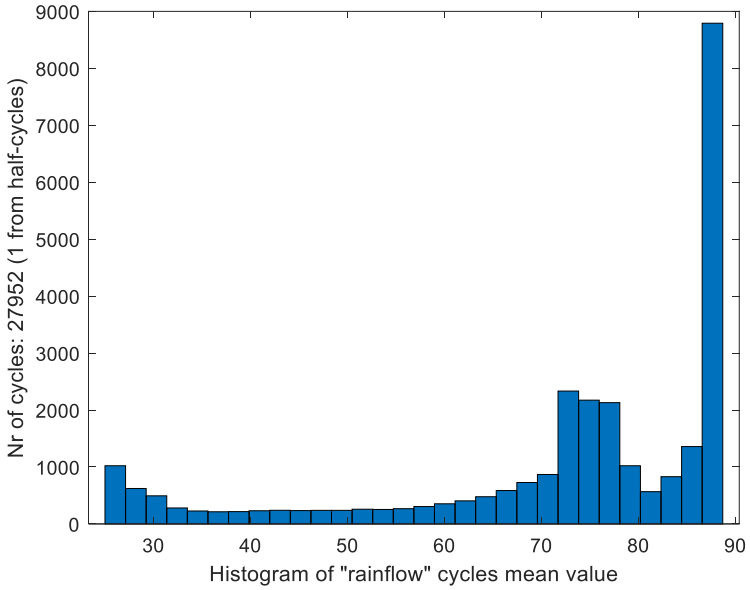

Figure B- 5 15kHz With Control

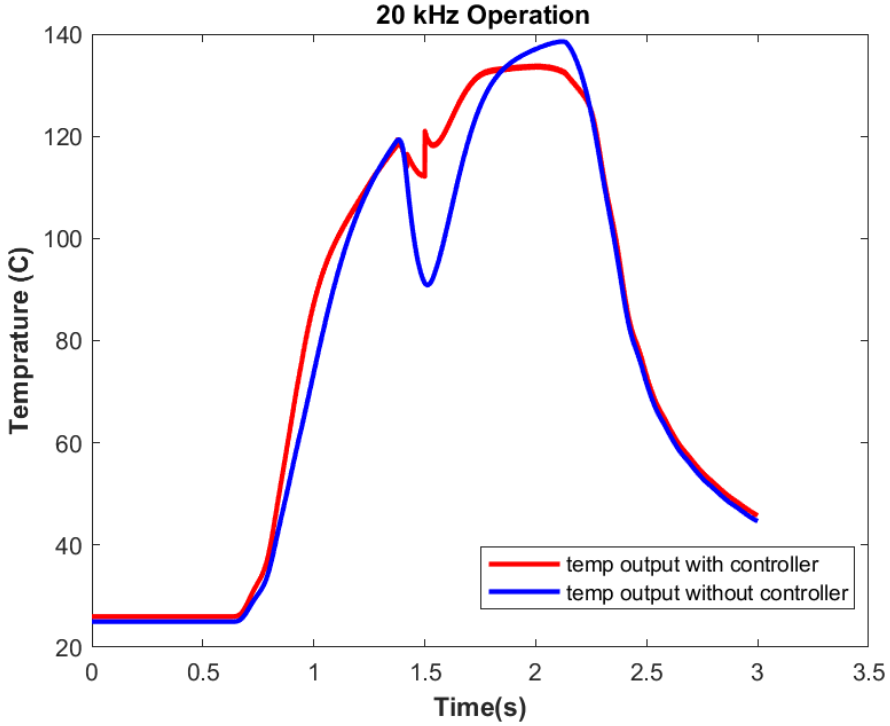

Figure B- 6 Temprature Graph at 20kHz

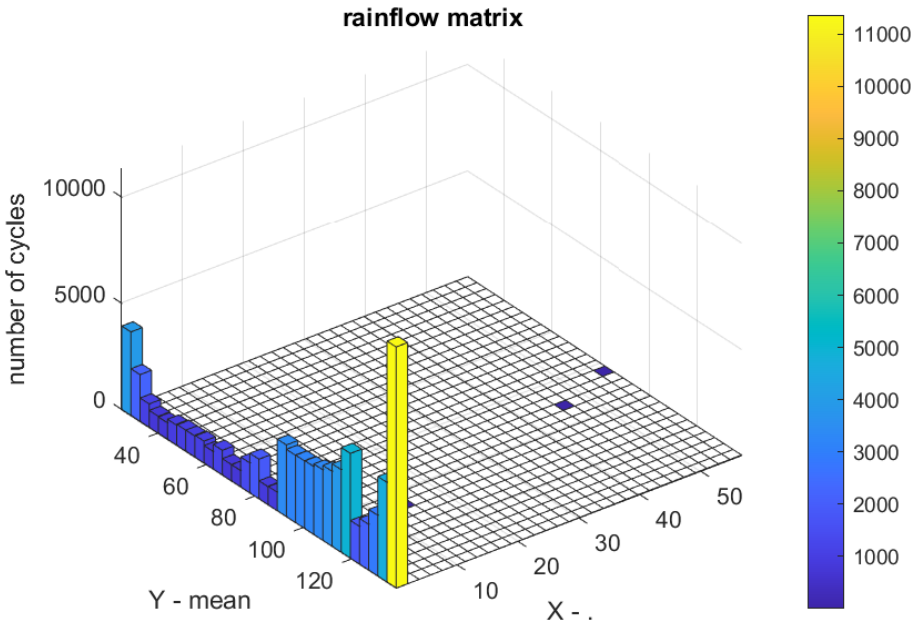

Figure B- 7 20kHz Without Control

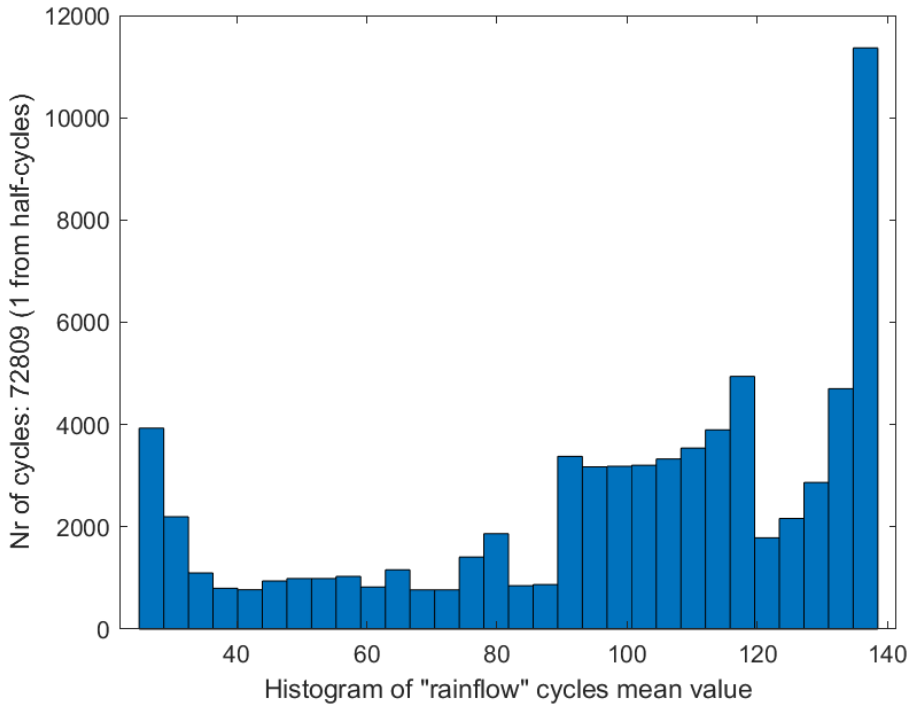

Figure B- 8 20kHz Without Control

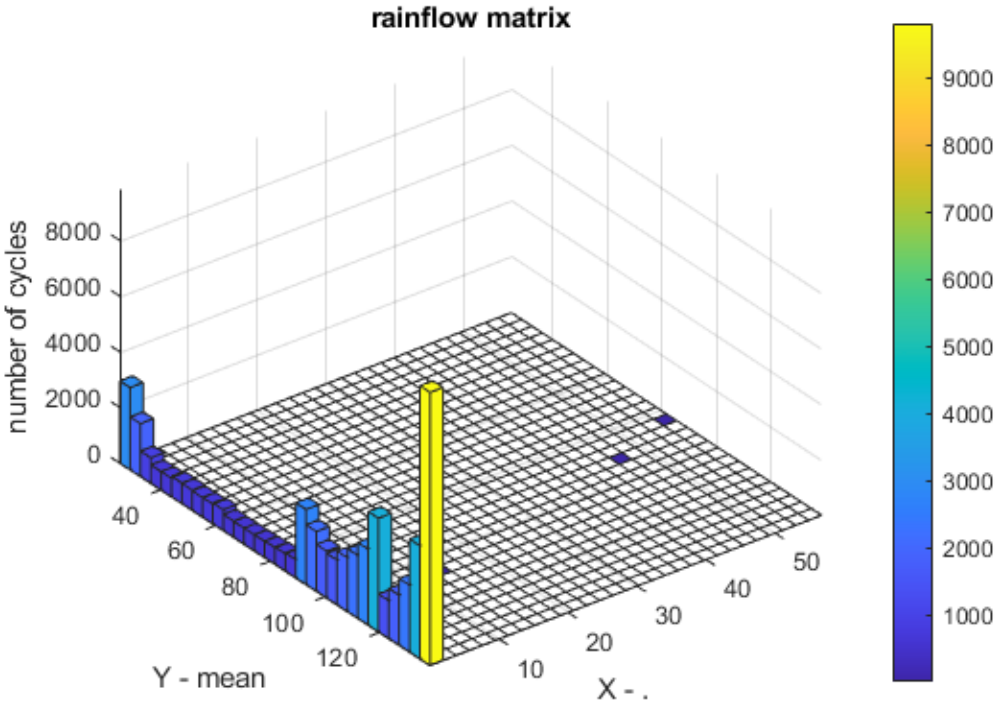

Figure B- 9 20kHz With Control

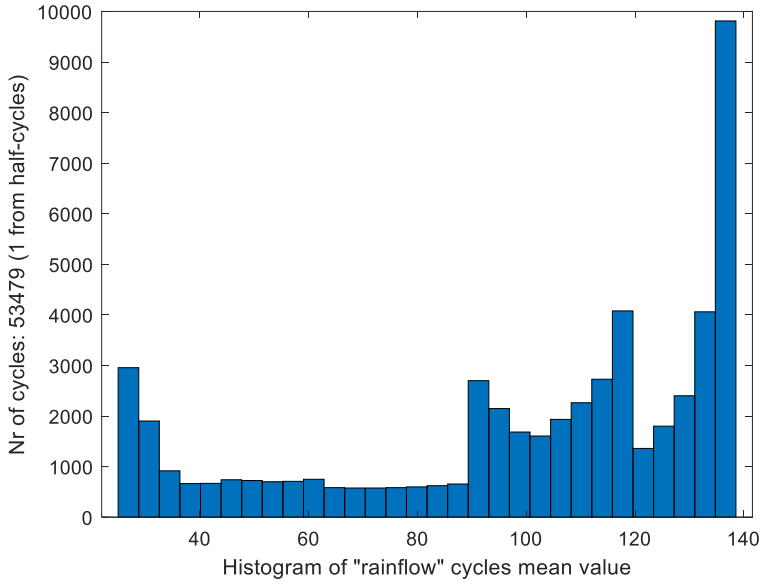

Figure B- 10 20Khz With Control

C. Indcutor Values for Different Duty Cycle, Frequency and Ripple Factor

		Ripple %				
		2	5	10	15	20
Frequency kHz	1	12.03509	4.814035	2.407018	1.604678	1.203509
	5	2.407018	0.962807	0.481404	0.320936	0.240702
	10	1.203509	0.481404	0.240702	0.160468	0.120351
	15	0.802339	0.320936	0.160468	0.106979	0.080234
	20	0.601754	0.240702	0.120351	0.080234	0.060175

Figure C- 1 Duty Cycle 0.4

		Ripple %				
		2	5	10	15	20
Frequency kHz	1	12.5	5	2.5	1.666667	1.25
	5	2.5	1	0.5	0.333333	0.25
	10	1.25	0.5	0.25	0.166667	0.125
	15	0.833333	0.333333	0.166667	0.111111	0.083333
	20	0.625	0.25	0.125	0.083333	0.0625

Figure C- 2 Duty Cycle 0.5

		Ripples %				
		2	5	10	15	20
Frequency kHz	1	12	4.8	2.4	1.6	1.2
	5	2.4	0.96	0.48	0.32	0.24
	10	1.2	0.48	0.24	0.16	0.12
	15	0.8	0.32	0.16	0.106667	0.08
	20	0.6	0.24	0.12	0.08	0.06

Figure C- 3 Duty Cycle 0.6

		Ripple %				
		2	5	10	15	20
Frequency kHz	1	10.5307	4.212281	2.10614	1.404094	1.05307
	5	2.10614	0.842456	0.421228	0.280819	0.210614
	10	1.05307	0.421228	0.210614	0.140409	0.105307
	15	0.702047	0.280819	0.140409	0.093606	0.070205
	20	0.526535	0.210614	0.105307	0.070205	0.052654

Figure C- 4 Duty Cycle 0.7